(also known as GRP78 or HSPA5) (Fig. 2*G*). These results suggested that ER stress response and UPR might be involved in the pathogenesis in SCN.

To examine further the differences in gene expression between the two cell types, a microarray analysis was carried out by using $CD34^+$ cells derived from SCN-iPS and control iPS cells (three clones of each) in suspension culture on day 2. At this early time point, differences in cell number and morphology were not yet readily discernible between SCN-iPS and control iPS cells, as shown in Fig. 2*A*. However, the microarray analysis revealed a differential expression of various genes between the two cell types. Transcription factor genes, which were related to neutrophil development [e.g., CCAAT/enhancer-binding protein (C/EBP)-α (20), C/EBP-β (21), C/EBP-ε (22), and SPI1 (also known as PU.1) (23)], were all down-regulated in SCN-iPS cells. B-cell chronic lymphocytic leukemia/lymphoma 2, which regulates cell death under ER stress through the core mitochondrial apoptosis pathway (24), was also down-regulated (Fig. 3*A*). These findings were confirmed by quantitative reverse-transcriptional PCR (qRT-PCR), as shown in Fig. 2*H*.

Notably, the down-regulation of the genes in SCN-iPS cells related to and regulated by the wingless-type mmtv integration site family, member 3a (Wnt3a)/β-catenin pathway [e.g., Wnt3a, lymphoid enhance-binding factor (LEF)-1, BIRC5 (also known as survivin), and cyclin D1] was also uncovered by microarray analysis and qRT-PCR (Fig. 3 *A–C* and Fig. S4). Therefore, we examined the effect of enhancement of Wnt3a/β-catenin signaling by exogenous Wnt3a addition on the neutrophil development of $CD34^+$ cells derived from SCN-iPS and control iPS cells. Although Wnt3a did not stimulate the survival, proliferation, and differentiation of $CD34^+$ cells derived from both iPS cells in the absence of cytokines stimulating myelopoiesis including G-CSF, the addition of Wnt3a to the neutrophil differentiation medium induced a dose-dependent increase in the percentage of mature neutrophils among the cultured cells, as shown in Fig. 3 *D* and *E*. Furthermore, when Wnt3a was added concurrently with 1,000ng/mL G-CSF, the proportion of mature neutrophils increased more than it did with Wnt3a or 1,000 ng/mL G-CSF alone, reaching a value comparable with that observed for control iPS cells (Fig. 4 *A* and *B*).

The reduced expression of LEF-1 (as regulated by the Wnt3a/β-catenin pathway) reportedly plays a critical role in the defective maturation of neutrophils in SCN patients (25). Therefore, we next examined LEF-1 mRNA expression in SCN-iPS–$CD34^+$ cells cultured in the presence of Wnt3a, G-CSF (1,000 ng/mL), or both. Wnt3a and G-CSF both enhanced LEF-1 mRNA expression, but the most significant increase was observed in the presence of Wnt3a plus G-CSF. LEF-1 expression in SCN-iPS–$CD34^+$ cells in response to Wnt3a plus G-CSF was almost the same as that in control iPS–$CD34^+$ cells (Fig. 4*C*). These results substantiate the importance of LEF-1 in neutrophil development and the pathogenesis of SCN, as shown (25). Moreover the

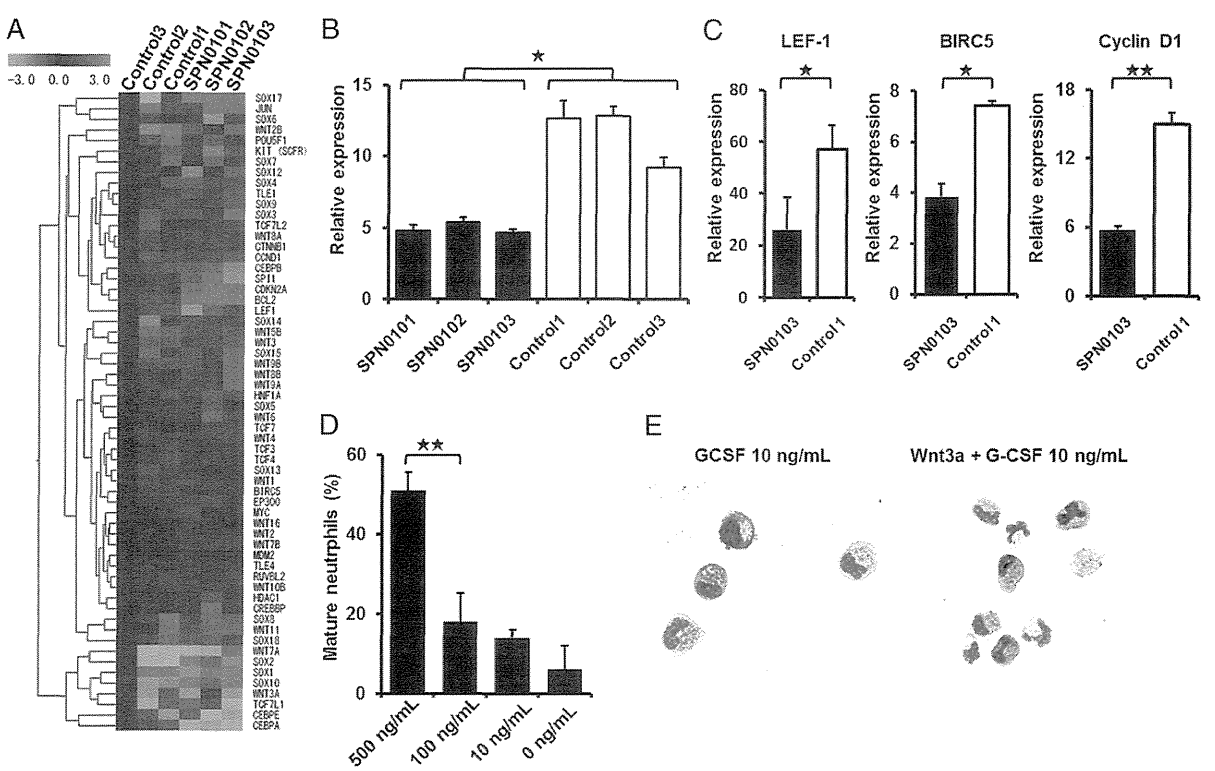

Fig. 3. Effects of Wnt3a on neutrophil development from SCN-iPS cells. (*A*) Heat map showing differential gene expression among SCN-iPS and control iPS cells on day 2. Red, high gene expression; blue, low gene expression compared with gene expression in control 3. (*B*) qRT-PCR analysis of the relative mRNA expression (target/HPRT expression) of Wnt3a on day 2. Filled and open bars indicate experiments using SCN-iPS cells (SPN0101, SPN0102, and SPN0103) and control iPS cells (controls 1, 2, and 3), respectively. Data are shown as mean ± SD. $^*P < 0.05$. (*C*) qRT-PCR analysis of the relative expression (target/HPRT expression) of genes regulated by the Wnt3a/β-catenin pathway (LEF-1, survivin, and cyclin D1) in SCN-iPS cells (filled bars, SPN0103) vs. control iPS cells (open bars, control 1) on day 2 of suspension culture. Data are shown as mean ± SD. $^{**}P < 0.01$; $^*P < 0.05$. (*D*) Proportion of mature neutrophils among the cells derived from SCN-iPS cells (SPN0102) on day 14 of suspension culture with dose escalation of Wnt3a. Data are shown as mean ± SD. $^{**}P < 0.01$. (*E*) Photographs of nonadherent cells on day 7 of suspension culture with or without Wnt3a (500 ng/mL) (400×; May–Grünwald–Giemsa staining).

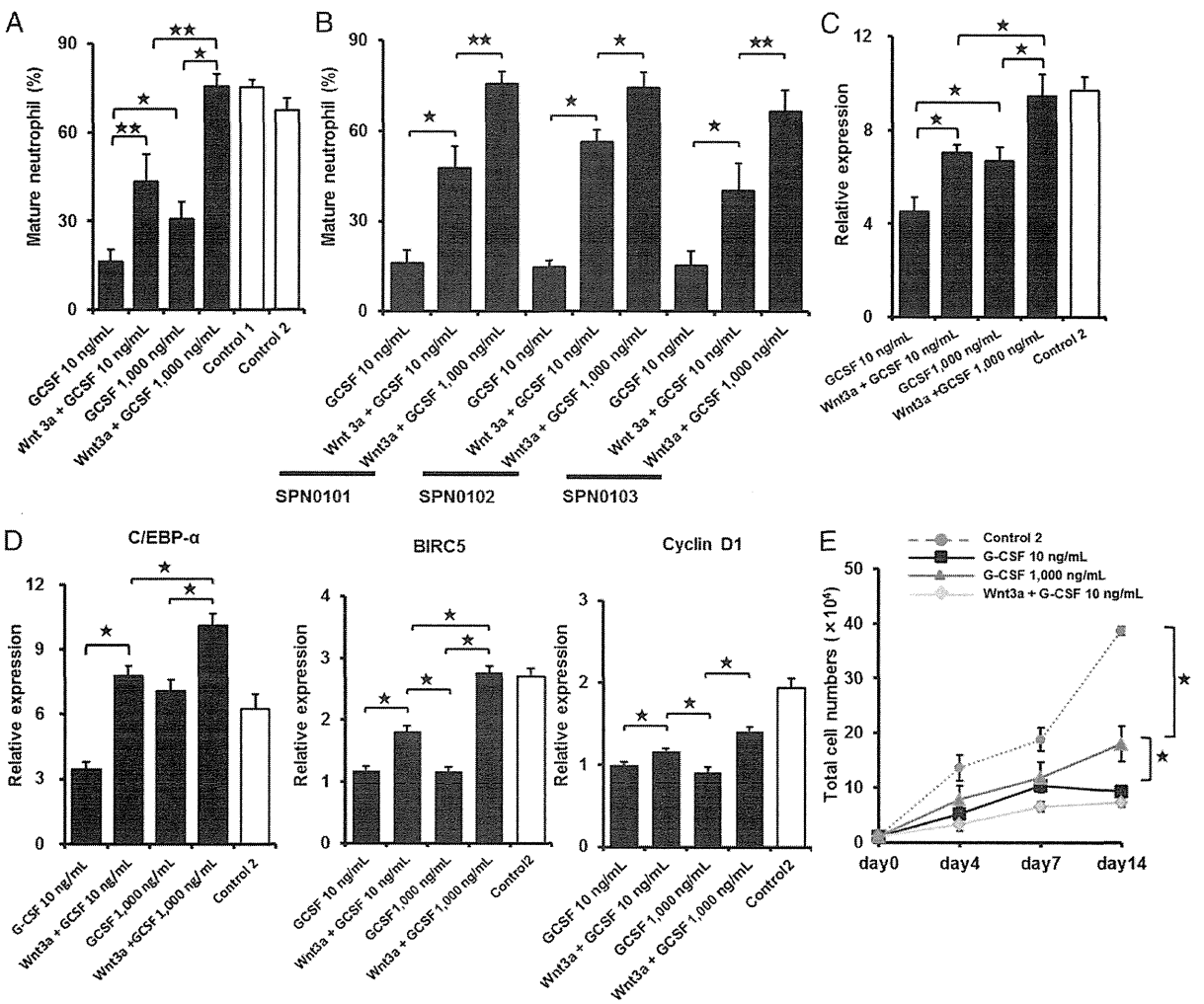

Fig. 4. Effects of Wnt3a in combination with high-dose G-CSF. (*A*) Filled and open bars show the proportion of mature neutrophils among the cells derived from SCN-iPS cells (SPN0101) on day 14 of suspension culture in the presence of neutrophil differentiation medium containing 10 ng/mL G-CSF (GCSF 10 ng/mL); 500 ng/mL Wnt3a and 10 ng/mL G-CSF (Wnt3a+GCSF 10 ng/mL); 1,000 ng/mL G-CSF (GCSF 1,000 ng/mL); or 500 ng/mL Wnt3a and 1,000 ng/mL G-CSF (Wnt3a + GCSF 1,000 ng/mL); and that from control iPS cells (controls 1 and 2) cultured in the neutrophil differentiation medium containing 10 ng/mL G-CSF, respectively. Data are shown as mean ± SD. $^{**}P < 0.01$; $^{*}P < 0.05$. (*B*) The proportion of mature neutrophils among the cells derived from three SCN-iPS cell clones (SPN0101, SPN0102, and SPN0103) on day 14 of suspension culture in the presence of neutrophil differentiation medium containing 10 ng/mL G-CSF (GCSF 10 ng/mL); 500 ng/mL Wnt3a and 10 ng/mL G-CSF (Wnt3a+GCSF 10 ng/mL); or 500 ng/mL Wnt3a and 1,000 ng/mL G-CSF (Wnt3a + GCSF 1,000 ng/mL). Data are shown as mean ± SD. $^{**}P < 0.01$; $^{*}P < 0.05$. (*C*) Filled and open bars show the relative expression (target/HPRT expression) of LEF-1 mRNA in SCN-iPS cells (SPN0101) on day 2 of suspension culture in the presence of differentiation medium containing the same combinations of Wnt3a and G-CSF as shown in *A* and that from control iPS cells (control 2), respectively. Data are shown as mean ± SD. $^{**}P < 0.01$; $^{*}P < 0.05$. (*D*) Filled and open bars show the relative expression (target/HPRT expression) of C/EBP-α, BIRC5, or cyclin D1 mRNA in SCN-iPS cells (SPN0101) on day 2 of suspension culture in the presence of differentiation medium containing the same combinations of Wnt3a and G-CSF as shown in *A* and that from control iPS cells (control 2), respectively. Data are shown as mean ± SD. $^{**}P < 0.01$; $^{*}P < 0.05$. (*E*) Total cell numbers of nonadherent cells in suspension cultures of 1×10^4 $CD34^+$ cells derived from control iPS cells (control 2; red broken line) and SCN-iPS cells (SPN0101) in the presence of neutrophil differentiation medium (black line) and those from SCN-iPS cells in the presence of neutrophil differentiation medium containing 500 ng/mL Wnt3a (yellow line) or 1,000 ng/mL G-CSF (black line). Data are shown as mean ± SD. $^{**}P < 0.05$.

administration of Wnt3a led to up-regulate C/EBP-α, cyclin D1, and BIRC5/survivin in addition to LEF-1 in the presence of G-CSF (Fig. 4*D*). These results suggested that the up-regulation of LEF-1 expression might promote granulopoiesis by increasing the expressions of cyclin D1, BIRC5/survivin, and C/EBP-α and its binding to LEF-1 in accordance with the previous report (25). Interestingly, Wnt3a did not stimulate the proliferation of myeloid cells, whereas 1,000 ng/mL G-CSF did to a certain extent (Fig. 4*E*). Hence, Wnt3a was capable of stimulating the maturation of impaired neutrophils in the presence of G-CSF, but not the proliferation of myeloid cells from SCN-iPS cells.

Importantly, aside from providing new insights into the mechanisms behind impaired neutrophil development in SCN patients, the present study demonstrates that agents activating the Wnt3a/β-catenin pathway are potential candidates for new drugs for SCN with mutations in the ELANE gene. Because endogenous G-CSF is readily increased in SCN patients (26), these activating agents may be viable alternatives to exogenous G-CSF treatment.

Materials and Methods

Additional information is available in *SI Materials and Methods*.

Generation of Human iPS Cells. BM fibroblasts from a patient with SCN and skin dermal fibroblasts from a healthy donor were acquired after obtaining informed consent after getting the approval by the Ethics Committee of the Institute of Medical Science, University of Tokyo, in accordance with the Declaration of Helsinki. The SCN patient presented with a heterozygous mutation in the ELANE gene in the 707 region of exon 5. SCN-iPS cells were established from the SCN-BM fibroblasts by transfection with the pMX retroviral vector, as described (10). This vector expressed the human transcription factors OCT3/4, SOX2, KLF4, and c-MYC. Control iPS cell clones, control 1 (TkDN4-M) and control 3 (201B7), were gifts from K. Eto and S. Yamanaka (Kyoto University, Kyoto), respectively (10, 11). Control 2 (SPH0101) was newly generated from another healthy donor's skin dermal fibroblasts by using the same methods.

Hematopoietic Colony Assay. A hematopoietic colony assay was performed in an aliquot of culture mixture, which contained 1.2% methylcellulose (Shin-Etsu Chemical), 30% (vol/vol) FBS, 1% (vol/vol) deionized fraction V BSA, 0.1 mM 2-mercaptoethanol (2-ME), α-minimum essential medium, and a cytokine mixture consisting of 100 ng/mL human stem cell factor (hSCF) (Wako), 100 ng/mL fusion protein 6 [FP6; a fusion protein of interleukin (IL)-6 and IL-6 receptor] (a gift from Tosoh), 10 ng/mL human IL-3 (hIL-3) (a gift from Kirin Brewery), 10 ng/mL human thrombopoietin (hTPO) (a gift from Kirin Brewery), 10 ng/mL human G-CSF (a gift from Chugai Pharmaceutical), and 5 U/mL human erythropoietin (a gift from Kirin Brewery). For dose escalation experiments, various concentrations (0, 1, 10, 100, and 1,000 ng/mL) of G-CSF were used instead of the cytokine mixture described above. Colony types were determined according to established criteria on day 14 of culture by in situ observations under an inverted microscope (IX70; Olympus) (27).

Suspension Culture and Neutrophil Differentiation Assay. $CD34^+$ cells (1×10^4 cells) were cocultured with irradiate confluent AGM-S3 cells in neutrophil differentiation medium containing Iscove's modified Dulbecco's medium, 10% FBS, 3 mM L-glutamine, 1×10^{-4} M 2-ME, 1×10^{-4} M nonessential amino acids solution, 100 ng/mL hSCF, 100 ng/mL FP6, 10 ng/mL hIL-3, 10 ng/mL hTPO, and 10 or 1,000 ng/mL human G-CSF. Wnt3a (10, 100, or 500 ng/mL) (R&D) was then added. The medium was replaced with an equivalent volume of fresh medium every 4 d. Living, nonadherent cells were counted following 0.4% trypan blue staining.

PCR primer. All primer sets used in this study are shown in Table S1.

Statistical Analysis. All data are presented as mean ± SD. $P < 0.05$ was considered significant. Statistical analyses were performed by using Prism software (GraphPad).

ACKNOWLEDGMENTS. We thank the individual with SCN who participated in this study; K. Eto for providing control iPS cells (control 1; TkDN4-M); S. Yamanaka for providing control iPS cells (control 3; 206B7); and E. Matsuzaka and S. Hanada for technical assistance. This work was supported by in part by Ministry of Education, Culture, Sports, Science, and Technology of Japan (MEXT) Grants-in-Aid (to Y.E.) and Project for Realization of Regenerative Medicine (MEXT) Grants-in-Aid (to K.Tsuji).

1. Zeidler C, Germeshausen M, Klein C, Welte K (2009) Clinical implications of *ELA2-, HAX1-,* and G-CSF-receptor (*CSF3R*) mutations in severe congenital neutropenia. *Br J Haematol* 144(4):459–467.
2. Freedman MH, et al. (2000) Myelodysplasia syndrome and acute myeloid leukemia in patients with congenital neutropenia receiving G-CSF therapy. *Blood* 96(2):429–436.
3. Dale DC, et al. (1993) A randomized controlled phase III trial of recombinant human granulocyte colony-stimulating factor (filgrastim) for treatment of severe chronic neutropenia. *Blood* 81(10):2496–2502.
4. Rosenberg PS, et al.; Severe Chronic Neutropenia International Registry (2006) The incidence of leukemia and mortality from sepsis in patients with severe congenital neutropenia receiving long-term G-CSF therapy. *Blood* 107(12):4628–4635.
5. Xia J, et al. (2009) Prevalence of mutations in ELANE, GFI1, HAX1, SBDS, WAS and G6PC3 in patients with severe congenital neutropenia. *Br J Haematol* 147(4):535–542.
6. Horwitz MS, et al. (2007) Neutrophil elastase in cyclic and severe congenital neutropenia. *Blood* 109(5):1817–1824.
7. Hajjar E, Broemstrup T, Kantari C, Witko-Sarsat V, Reuter N (2010) Structures of human proteinase 3 and neutrophil elastase—so similar yet so different. *FEBS J* 277(10): 2238–2254.
8. Fouret P, et al. (1989) Expression of the neutrophil elastase gene during human bone marrow cell differentiation. *J Exp Med* 169(3):833–845.
9. Pham CT (2006) Neutrophil serine proteases: Specific regulators of inflammation. *Nat Rev Immunol* 6(7):541–550.
10. Takayama N, et al. (2010) Transient activation of c-MYC expression is critical for efficient platelet generation from human induced pluripotent stem cells. *J Exp Med* 207(13):2817–2830.
11. Takahashi K, et al. (2007) Induction of pluripotent stem cells from adult human fibroblasts by defined factors. *Cell* 131(5):861–872.
12. Germeshausen M, Ballmaier M, Welte K (2007) Incidence of CSF3R mutations in severe congenital neutropenia and relevance for leukemogenesis: Results of a long-term survey. *Blood* 109(1):93–99.
13. Ma F, et al. (2007) Novel method for efficient production of multipotential hematopoietic progenitors from human embryonic stem cells. *Int J Hematol* 85(5):371–379.
14. Konishi N, et al. (1999) Defective proliferation of primitive myeloid progenitor cells in patients with severe congenital neutropenia. *Blood* 94(12):4077–4083.
15. Nakamura K, et al. (2000) Abnormalities of primitive myeloid progenitor cells expressing granulocyte colony-stimulating factor receptor in patients with severe congenital neutropenia. *Blood* 96(13):4366–4369.
16. Skokowa J, Fobiwe JP, Dan L, Thakur BK, Welte K (2009) Neutrophil elastase is severely down-regulated in severe congenital neutropenia independent of ELA2 or HAX1 mutations but dependent on LEF-1. *Blood* 114(14):3044–3051.
17. Kawaguchi H, et al. (2003) Dysregulation of transcriptions in primary granule constituents during myeloid proliferation and differentiation in patients with severe congenital neutropenia. *J Leukoc Biol* 73(2):225–234.
18. Köllner I, et al. (2006) Mutations in neutrophil elastase causing congenital neutropenia lead to cytoplasmic protein accumulation and induction of the unfolded protein response. *Blood* 108(2):493–500.
19. Grenda DS, et al. (2007) Mutations of the ELA2 gene found in patients with severe congenital neutropenia induce the unfolded protein response and cellular apoptosis. *Blood* 110(13):4179–4187.
20. Pabst T, et al. (2001) AML1-ETO downregulates the granulocytic differentiation factor C/EBPalpha in t(8;21) myeloid leukemia. *Nat Med* 7(4):444–451.
21. Hirai H, et al. (2006) C/EBPbeta is required for 'emergency' granulopoiesis. *Nat Immunol* 7(7):732–739.
22. Bedi R, Du J, Sharma AK, Gomes I, Ackerman SJ (2009) Human C/EBP-ε activator and repressor isoforms differentially reprogram myeloid lineage commitment and differentiation. *Blood* 113(2):317–327.
23. Friedman AD (2007) Transcriptional control of granulocyte and monocyte development. *Oncogene* 26(47):6816–6828.
24. Hetz C (2012) The unfolded protein response: Controlling cell fate decisions under ER stress and beyond. *Nat Rev Mol Cell Biol* 13(2):89–102.
25. Skokowa J, et al. (2006) LEF-1 is crucial for neutrophil granulocytopoiesis and its expression is severely reduced in congenital neutropenia. *Nat Med* 12(10):1191–1197.
26. Mempel K, Pietsch T, Menzel T, Zeidler C, Welte K (1991) Increased serum levels of granulocyte colony-stimulating factor in patients with severe congenital neutropenia. *Blood* 77(9):1919–1922.
27. Nakahata T, Ogawa M (1982) Hemopoietic colony-forming cells in umbilical cord blood with extensive capability to generate mono- and multipotential hemopoietic progenitors. *J Clin Invest* 70(6):1324–1328.

bjh research paper

Identification of the integrin β3 L718P mutation in a pedigree with autosomal dominant thrombocytopenia with anisocytosis

Yoshiyuki Kobayashi,[1,2] Hirotaka Matsui,[1]* Akinori Kanai,[1] Miyuki Tsumura,[2] Satoshi Okada,[2] Mizuka Miki,[2] Kazuhiro Nakamura,[2] Shinji Kunishima,[3] Toshiya Inaba[1] and Masao Kobayashi[2]

[1]Department of Molecular Oncology and Leukaemia Programme Project, Research Institute for Radiation Biology and Medicine, Hiroshima University, [2]Department of Paediatrics, Graduate School of Biomedical and Health Sciences, Hiroshima University, Minami-ku, Hiroshima, and [3]Department of Advanced Diagnosis, Clinical Research Centre, National Hospital Organization Nagoya Medical Centre, Nagoya, Aichi, Japan

Received 29 June 2012; accepted for publication 22 October 2012

Correspondence: Hirotaka Matsui, Department of Molecular Oncology and Leukemia Program Project, Research Institute for Radiation Biology and Medicine, Hiroshima University, 1-2-3 Kasumi, Minami-ku, Hiroshima 734-8553, Japan.
E-mail: hmatsui@hiroshima-u.ac.jp

Summary

αIIbβ3 integrin mutations that result in the complete loss of expression of this molecule on the platelet surface cause Glanzmann thrombasthenia. This is usually autosomal recessive, while other mutations are known to cause dominantly inherited macrothrombocytopenia (although such cases are rare). Here, we report a 4-generation pedigree including 10 individuals affected by dominantly inherited thrombocytopenia with anisocytosis. Six individuals, whose detailed clinical and laboratory data were available, carried a non-synonymous *ITGB3* gene alteration resulting in mutated integrin β3 (ITGB3)-L718P. This mutation causes partial activation of the αIIbβ3 complex, which promotes the generation of abnormal pro-platelet-like protrusions through downregulating RhoA (RHOA) activity in transfected Chinese Hamster Ovary cells. These findings suggest a model whereby the integrin β3-L718P mutation contributes to thrombocytopenia through gain-of-function mechanisms.

Keywords: integrin β3 L718P mutation, familial thrombocytopenia, autosomal dominant inheritance, whole exome sequencing, inhibition of RhoA.

Lifelong haemorrhagic syndromes are in part caused by point mutations in the *ITGA2B* and *ITGB3* genes encoding ITGA2B and ITGB3 proteins (integrin αIIb and β3, respectively). The αIIbβ3 complex regulates thrombopoiesis by megakaryocytes and aggregation of platelets in response to extracellular stimuli, such as ADP and collagen. The autosomal recessive syndrome, Glanzmann thrombasthenia, is the most frequently encountered disease caused by αIIbβ3 mutations (George *et al*, 1990; Nurden, 2006; Nurden & Nurden, 2008; Nurden *et al*, 2011a). Patients have a homozygous or a compound heterozygous mutation in the *ITGA2B* or *ITGB3* genes that causes loss of function of the αIIbβ3 complex. Although platelet counts and size are generally normal, patients typically have severe mucocutaneous bleeding, such as epistaxis, menorrhagia and gastrointestinal bleeding, frequently because of defects in platelet aggregation.

Mutations of the αIIbβ3 complex are also involved in congenital haemorrhagic diseases other than Glanzmann thrombasthenia (Ghevaert *et al*, 2008; Schaffner-Reckinger *et al*, 2009; Jayo *et al*, 2010; Kunishima *et al*, 2011; Nurden *et al*, 2011b). For example, the integrin β3 D723H mutation is found in autosomal dominant macrothrombocytopenia (Ghevaert *et al*, 2008). Biochemical analysis revealed that integrin β3-D723H is a gain of function mutation which activates the αIIbβ3 complex constitutively, albeit only partially. This results in the formation of proplatelet-like protrusions in transfected Chinese Hamster Ovary (CHO) cells, a model of relevance for the formation of macrothrombocytes (Ghevaert *et al*, 2008; Schaffner-Reckinger *et al*, 2009).

More recently, a sporadic patient carrying an integrin β3-L718P mutation was reported (Jayo *et al*, 2010). She had mild thrombocytopenia (127×10^9/l), platelet anisocytosis and reduced platelet aggregation potential. This mutation also induces abnormal proplatelet formation.

In the present study, we report a pedigree with a total 10 of individuals affected by a dominantly inherited haemorrhagic

First published online 17 December 2012
doi:10.1111/bjh.12160

syndrome. Six individuals whose detailed clinical and laboratory data are available, presented with thrombocytopenia accompanied by anisocytosis and carry a non-synonymous *ITGB3* T2231C alteration resulting in the integrin β3-L718P mutation. We also performed entire exon sequencing by a next-generation sequencing and found that the integrin β3-L718P mutation is most likely the sole gene responsible for thrombocytopenia in this pedigree.

Materials and methods

Written informed consent was obtained from individuals in the family in accordance with the Declaration of Helsinki for blood sampling and analysis undertaken with the approval of the Hiroshima University Institutional Review Board.

Patient

The patient was 4-year-old Japanese girl (iv.3 in Fig 1A), who presented with mild bleeding tendencies, such as recurrent nasal bleeding and purpura in her extremities. Her platelet count was 49–72 × 10^9/l with a mean platelet volume (MPV) of 9·8–10·9 fl. White blood cell and red blood cell counts were within the normal range and there were no morphological abnormalities including inclusions in neutrophils. Bone marrow examination was not performed. A total of six of her relatives, namely her father (iii.2), sister and brother (iv.1 and iv.2), two cousins (iv.4 and iv.5) and an aunt (iii.5), were subsequently found to have low platelet counts and were referred to our institute for further investigation.

Antibodies and reagents

Unconjugated or phycoerythrin-cyanin 5 (PC5)-conjugated anti-CD41 monoclonal antibody (Ab) (clone P2) against the αIIbβ3 complex (Beckman Coulter, Brea, CA, USA), fluorescein isothiocyanate (FITC)-conjugated anti-CD41a monoclonal Ab (clone HIP8) (Beckman Coulter), FITC- or peridinin chlorophyll (PerCP)-conjugated anti-CD61 monoclonal Ab (clone RUU-PL 7F12) (BD Biosciences, San Jose, CA, USA), FITC-conjugated PAC-1 (BD Biosciences) and Alexa488-conjugated human fibrinogen (Life Technologies, Carlsbad, CA, USA) were used in flow cytometry. Anti-CD61 monoclonal Ab (clone EP2417Y) (Abcam, Cambridge, UK), anti-DDDDK-tag polyclonal Ab (Medical & Biological Laboratories, Nagoya, Japan), Alexa488-conjugated phalloidin and Hoechst 33342 (both Life Technologies) were used for immunofluorescence microscopy. The oligopeptide Arg-Gly-Asp-Ser (RGDS) (Sigma–Aldrich, St Louis, MO, USA) was used to competitively inhibit the binding of ligands to αIIbβ3, and adenosine diphosphate (ADP) (nacalai tesque, Kyoto, Japan) was used for the stimulation of αIIbβ3 on platelets.

Construction and transfection of expression vectors

Full-length wild type (WT) *ITGA2B* and *ITGB3* cDNA were amplified by polymerase chain reaction (PCR) and cloned into pcDNA3·1 expression vectors. A PCR-mediated site-directed mutagenesis technique was applied to produce *ITGB3* mutants encoding integrin β3-L718P, -D723H and -T562N with or without truncation at the C-terminal side of Y^{759} (del. 759). *RHOA* cDNA, which encodes RhoA (RHOA) protein, was amplified by PCR and its mutants (T19N and Q63L) were generated by site-directed mutagenesis, followed by cloning into p3xFLAG-CMV-10 vectors (Sigma–Aldrich). The *ITGA2B* and *ITGB3* expression vectors were simultaneously transfected into CHO cells cultured in Ham's F12 medium supplemented with 10% fetal bovine serum at 37°C, in 5% CO_2, using Lipofectamine LTX reagent (Life Technologies) according to the manufacturer's instructions.

Immunofluorescent laser-scanning confocal microscopy

Cells grown on coverslips coated with 100 μg/ml fibrinogen were fixed with 4% paraformaldehyde, followed by permeabilization with phosphate-buffered saline containing 0·1% Triton X100. After blocking, the cells were stained with primary antibodies at appropriate dilutions, followed by staining with Alexa488- or *Cy3*-conjugated secondary antibodies together with Hoechst 33342. High-resolution immunofluorescent images were taken under a laser-scanning confocal microscopy (LSM5 Pascal, Carl Zeiss, Oberkochen, Germany) using a x63 objective.

Flow cytometry

The expression and activation of integrin αIIb and β3 on the platelet surface was indirectly estimated by flow cytometry with the antibodies described above. Mean fluorescence intensity (MFI) of values in an affected individual were divided by those in an unrelated normal control and recorded as relative MFI value (%). For the quantitative determination of αIIbβ3 molecules on the platelet surface, QIFIKIT (Dako, Glostrup, Denmark) was used according to the manufacturer's instructions. MFI of the calibration beads containing five populations (antibody-binding capacity: 2600, 9900, 46 000, 221 000 and 741 000) were 16·12, 63·83, 262·84, 1483·2 and 3772·1, respectively, whereas that of the negative control sample was 1·62. Therefore, αIIbβ3 molecules (copies/platelet) was calculated as $10^{(1.022 \times \log(\mathrm{MFI}) + 2.1679)} - 241$. Activation of platelets and CHO cells was estimated by methods previously described (Shattil *et al*, 1987; Hughes *et al*, 1996). Activation index was defined as $(F-F_0) / (F'-F_0)$, where F is the MFI of PAC-1-stained CHO cells transfected with αIIbβ3-L718P or αIIbβ3-D723H, and F_0 and F' are those transfected with αIIbβ3-WT and αIIbβ3-T562N, respectively. The samples were analyzed on a FACS Calibur (Becton Dickinson, Franklin Lakes, NJ, USA), equipped with an argon laser operating at 488 nm.

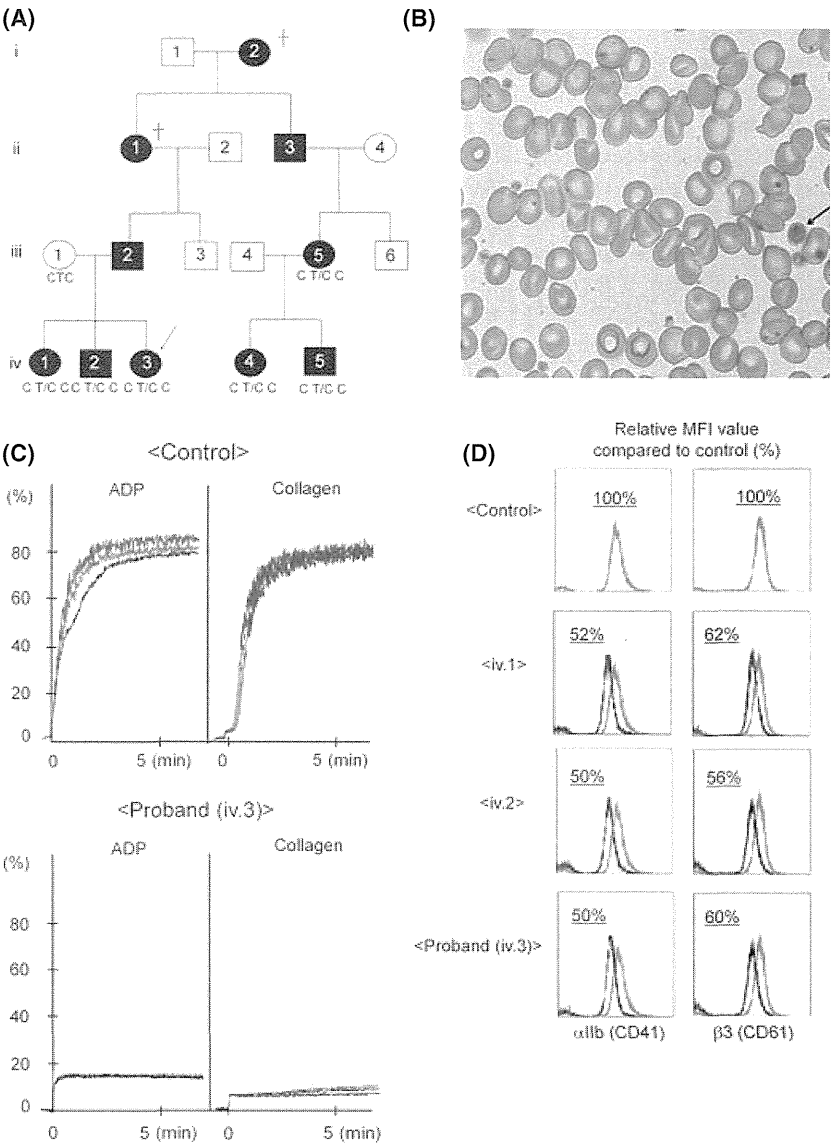

Fig 1. Platelet morphology and aggregation tracings. (A) The pedigree shows affected (filled) and unaffected (open) females (circles) and males (squares). The patient is indicated by an arrow. (B) Platelet morphology as determined by optical microscopy. Peripheral blood specimen obtained from the patient stained with May-Giemsa. The arrow indicates a macrothrombocyte. Original magnification × 600. (C) Representative platelet aggregation tracings in response to ADP and collagen stimuli in platelet-rich plasma from the patient and an unrelated normal control. (D) Flow cytometry of surface integrin αIIb (CD41) and β3 (CD61) expression. Samples were obtained from three affected individuals of the pedigree and an unrelated normal control. Data were calculated as relative MFI value (%), where MFIs of affected individuals were divided by MFI of a control sample.

Exome sequencing

Genomic DNA was obtained from four affected individuals in the pedigree and whole exome sequencing was performed. Briefly, 3 μg genomic DNA was fragmented by Covaris S2 (Covaris, Woburn, MA, USA) and ligated to adaptors, followed by hybridization to biotinylated RNA baits according to the manufacturer's instruction (Agilent Technologies, Santa Clara, CA, USA). The generated sequence tags were sequenced by the 76 bp paired-end protocol of Illumina GAIIx (Illumina, San Diego, CA, USA) and mapped onto the human genomic sequence (hg18, UCSC Genome Browser) using the sequence alignment program Eland (Illumina). Unmapped or redundantly mapped sequences were removed from the data set, and only uniquely mapped sequences were used for further analyses. Positions relative to RefSeq genes were calculated based on the respective genomic coordinates. Genomic coordinates of exons and the protein-coding regions of the RefSeq transcripts are as described in hg18. To verify the presence of *ITGB3* gene alteration, amplification and direct sequencing of a part of exon 14 was performed with the following primers; 5′-CATAGCCAGTTCAAGTGACTCCTG-3′ for forward primer and 5′-ACGATGGTACTGGCTGAACATGAC-3′ for reverse primer.

Results

Pedigree of a family with autosomal dominant thrombocytopenia with anisocytosis

In the original patient, marked platelet anisocytosis was observed in peripheral blood samples (Fig 1B). Platelet aggregation induced by ADP (1–4 μmol/l) and collagen (0·5–2 μg/ml) was markedly reduced (Fig. 1C and Table I), but agglutination induced by ristocetin (1·25 mg/ml) was within

the normal range (data not shown). Three affected individuals (iii.5, iv.1, and iv.2) showed abnormalities in platelet function similar to those of the original patient. In these affected individuals, the αIIb and β3 expression levels, which were indirectly estimated as relative MFI value (%), were 43–75% of a healthy control (Fig 1D and Table I). The number of αIIbβ3 molecules on the platelet surface in patients, as evaluated by flow cytometry using QIFIKIT, was 35 000–38 400 copies/platelet (MFI: 212·1 –232·4), whereas in an unaffected individual of the pedigree (iii.1) and an unrelated control, there were 65 200 and 62 100 copies/platelet (MFI: 389·2 and 371·3), respectively (Table I). The tendency to bleed was mild to moderate, as exemplified by the following episodes: when family member iv.1 received a bruise to the face, treatment with recombinant Factor VIIa was required because of persistent epistaxis; also, family member iii.5 had had to give birth by Caesarean section because of low platelet count. The family pedigree (Fig 1A), which shows no evidence of consanguineous marriage, strongly suggests the inheritance of thrombocytopenia as an autosomal dominant trait. The laboratory findings are shown in Table I.

Identification of the integrin β3 L718P mutation by whole exome analysis

To isolate a candidate gene alteration responsible for the thrombocytopenia, whole exome sequencing analysis was performed using genomic DNA obtained from the patient (iv.3), her sister and brother (iv.1 and iv.2) and a cousin (iv.4). A total of 794 non-synonymous gene alterations among 1551 SNPs that are not registered in dbSNP 129/130 were detected in the patient. To isolate the responsible gene, we selected non-synonymous gene alterations shared by the four affected individuals as strong candidates. Among the 90 alterations commonly found in the affected individuals of the pedigree (individual numbers of SNPs/mutations are shown in Table II), we focused on the heterozygous non-synonymous T2231C alteration in exon 14 of the *ITGB3* gene, which results in the substitution of leucine at 718 for proline (L718P) in the integrin β3 protein. We selected this because it was recently reported as a candidate mutation responsible for thrombocytopenia (Jayo *et al*, 2010). The presence of the mutation in six affected individuals of the pedigree (iv.1, iv.2, iv.3, iv.4, iii.5 and iv.5) and its absence in an unaffected individual (iii.1) and an unrelated control was confirmed by a direct-sequencing (Fig 2). As far as we could determine, no other non-synonymous gene alterations previously reported to cause thrombocytopenia or defective platelet function were present in the affected individuals of the pedigree. In addition, the L718 residue in integrin β3 is well-conserved between species and amino acid substitution in this position is predicted by bioinformatic tools, including Polyphen and SIFT, to cause a significant change in protein structure and function (data not shown). These observations strongly suggest that the L718P mutation in integrin β3 is the responsible gene alteration that causes familial thrombocytopenia.

Constitutive but partial activation of the αIIbβ3 complex by β3-L718P

To elucidate the effects of the integrin β3-L718P mutation on the activation status of αIIbβ3 complexes in resting or ADP-activated platelets, fresh platelets were analysed by flow cytometry using PAC-1, a ligand-mimicking antibody that specifically recognizes the activated form of the αIIbβ3 complex (Shattil *et al*, 1987).

Resting control platelets from healthy individuals bound PAC-1 with a similar affinity to those treated with RGDS, a peptide which competitively inhibits the binding of ligands for

Table I. Laboratory data of seven individuals of the pedigree.

						Relative MFI value compared to control (%)		αIIbβ3 molecules		Platelet aggregation (%)	
Patient	Sex	Age (years)	Platelet count ($\times 10^9$/l)	MPV (fl)	PDW (%)	αIIb	β3	MFI	copies/platelet	ADP (4 μM)	collagen (2·0 μg/ml)
iii.1	F	37	210	10·2	12·1	110	111	389·2	65 200	NA	NA
iii.5	F	34	38–67	8·5–11·3	10·0–19·0	43	75	NA	NA	15	12
iv.1	F	11	30–43	7·8–11·2	9·7–16·3	52	62	232·4	38 400	16	8
iv.2	M	8	49–64	10·3–11·1	10·1–14·7	50	56	216·4	35 700	23	16
iv.3	F	6	49–72	9·8–10·9	11·1–13·3	50	60	212·1	35 000	12	8
iv.4	F	4	32–59	9·9–10·8	12·3–15·6	NA	NA	NA	NA	NA	NA
iv.5	M	2	28–50	8·9–9·0	18·0–18·4	49	51	NA	NA	NA	NA

MPV, mean platelet volume (normal range: 9·4–12·3 fl); PDW, platelet distribution width (normal range: 9·5–14·8 %); NA, not available. αIIbβ3 molecules (copies/platelet) were calculated as $10^{(1\cdot022 \times \log(\mathrm{MFI}) + 2\cdot1679)} - 241$ (see *Materials and methods*).

Table II. Number of SNPs/mutations detected by whole exome sequencing.

Case	iv.1	iv.2	iv.3	iv.4
SNP	21 531	21 697	20 413	20 113
Not in dbSNP 129 and 130	1 674	1 722	1 473	1 551
Non-synonymous alternations				
Homozygous	62	58	65	42
Heterozygous	800	815	667	752
Non-synonymous (common)	90			

αIIbβ3 complex such as fibrinogen and PAC-1 (Fig 3A, compare black and blue lines), indicating that wild-type αIIbβ3 in resting platelets is not activated. In contrast, platelets obtained from the affected individuals (iii.5, iv.1, iv.2 and iv.3) showed a slight increase of PAC-1 binding compared to those treated with RGDS (Fig 3A). Indeed, resting platelets from affected individuals showed a slight but significant increase of PAC-1 binding relative to healthy individuals (Fig 3A, top panel). In addition, flow cytometric analysis using FITC-conjugated fibrinogen also showed a significant increase of fibrinogen binding potential in resting platelets from affected individuals compared with healthy controls (bottom panel). Because MPV (shown in Table I) did not exceed the normal range (9·4–12·3 fl) and surface expression levels of αIIbβ3 were lower in patients than controls (Fig 1D), it is proposed that these observations indicate spontaneous activation of αIIbβ3-L718P in resting platelets.

ADP-activated platelets from healthy volunteers, on the other hand, bound to PAC-1 with a very high affinity (Fig 3B, red lines and 3B, top panel), as expected. In contrast, only a small increase of affinity to PAC-1 was observed in ADP-treated platelets carrying the β3-L718P mutation, resulting in a marginal increase of binding potential (bottom panel). These findings suggest that αIIbβ3-L718P is partially activated in the absence of inside-out signals such as ADP, but nevertheless cannot be fully activated in the presence of such signals.

To confirm the contribution of the integrin β3-L718P mutation to spontaneous activation of αIIbβ3, CHO cells were transiently transfected with expression vectors encoding integrin β3-WT, -L718P, -D723H or -T562N together with a vector encoding αIIb-WT. Flow cytometric analysis (Fig 3C) revealed that αIIbβ3-L718P expressed in CHO cells bound to PAC-1 to the same degree as αIIbβ3-D723H, a mutant previously reported to partially activate αIIbβ3, and to a lesser extent than a fully active αIIbβ3-T562N mutant (Kashiwagi *et al*, 1999). We calculated the activation indices (see *Materials and methods*) (Hughes *et al*, 1996; Schaffner-Reckinger *et al*, 2009) of αIIbβ3-L718P and -D723H as 0·23 ± 0·07 and 0·16 ± 0·02, respectively, taking αIIbβ3-T562N as fully active (=1·0) and αIIbβ3-WT as inactive (=0) (Fig 3D). Because CHO cells were not stimulated by ADP in this experiment, each index represents αIIbβ3 activation status at rest.

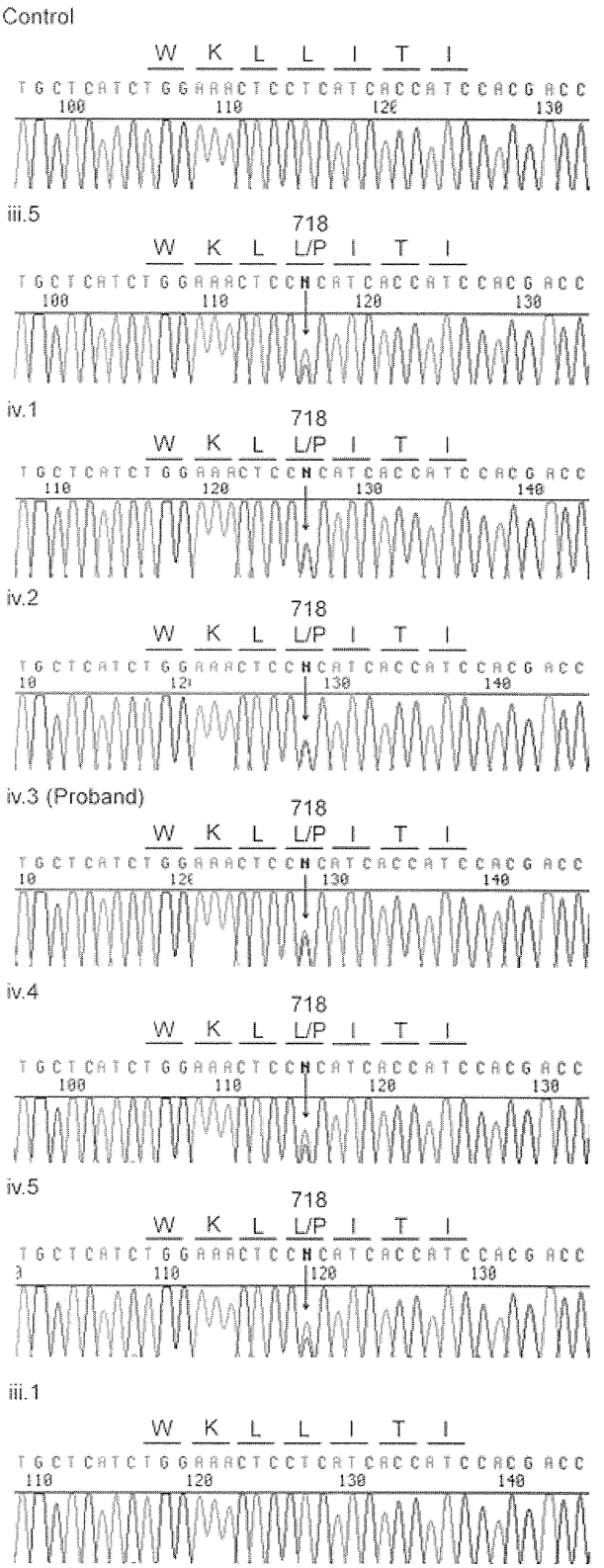

Fig 2. Direct sequencing analysis around T2231 in exon 14 of the *ITGB3* gene. Genomic DNA extracted from the affected and unaffected individuals of the pedigree were amplified by polymerase chain reaction and sequenced. Arrows indicate the position of the T2231 mutation in the *ITGB3* gene.

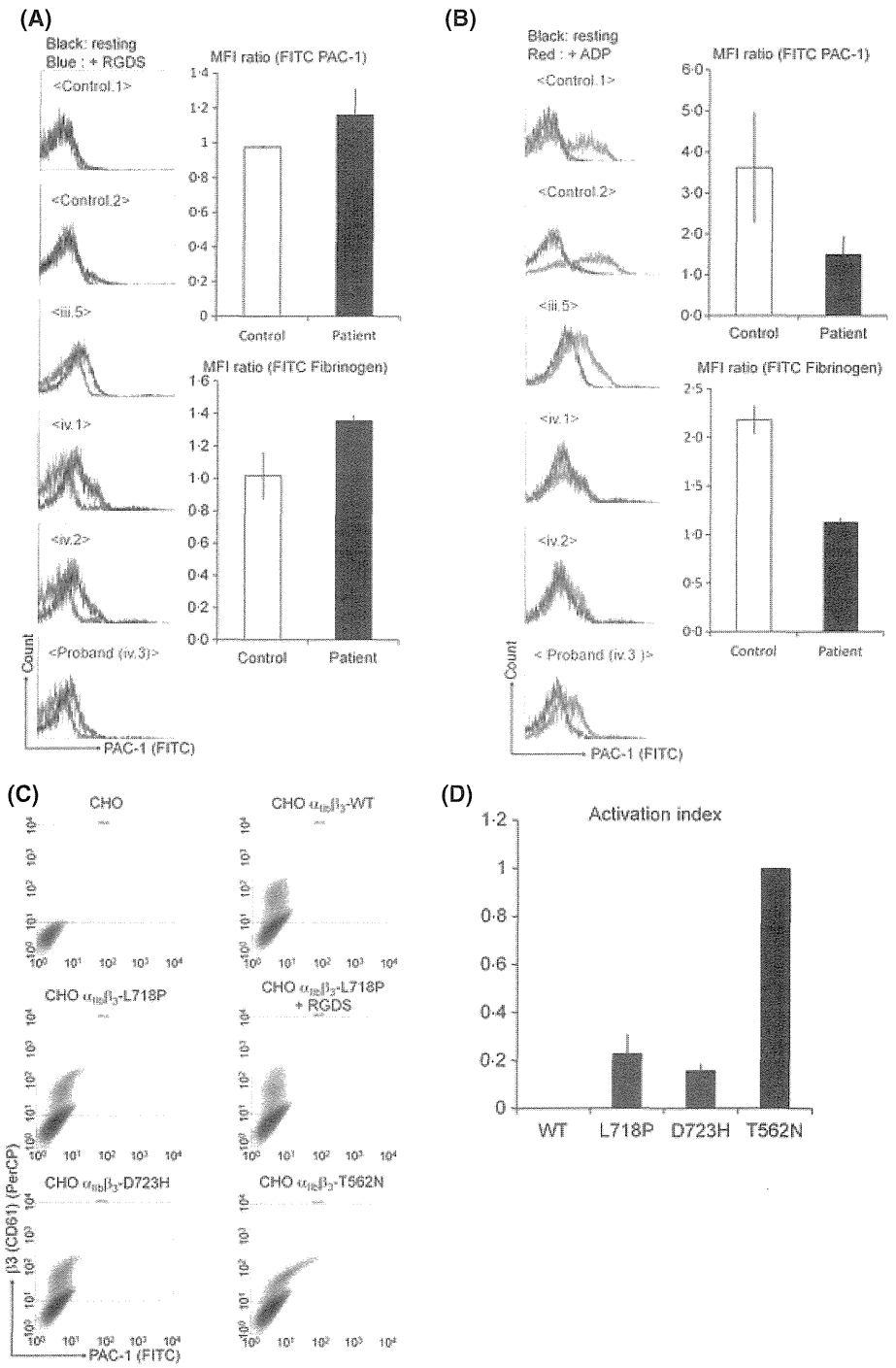

Fig 3. Functional analysis of integrin β3-L718P mutation. (A) Spontaneous binding of PAC-1 antibody to platelets obtained from affected individuals of the pedigree. Non-activated platelets (within 10 min after blood collection), incubated with or without 1 mM RGDS, were stained with FITC-conjugated PAC-1 antibody. After fixation, binding of PAC-1 to platelets was analysed by flow cytometry. Activation status of αIIbβ3 complex on resting platelets bound to FITC-PAC-1 (top) and FITC-fibrinogen (bottom). Mean fluorescence intensity (MFI) ratio was estimated by dividing the MFI of resting platelets by that of resting platelets incubated with RGDS. (B) Reduced activation of αIIbβ3 from affected individuals. The resting and ADP-stimulated platelets, stained with FITC-conjugated PAC-1 antibody were analysed by flow cytometry. Activation status of αIIbβ3 on stimulated platelets bound to FITC-PAC-1 (top) and FITC-fibrinogen (bottom). Values were estimated by dividing the MFI of platelets stimulated with ADP by those of resting platelets. (C) Partial activation of αIIbβ3-L718P and -D723H on CHO cells. CHO cells transfected with αIIbβ3 expression vectors (β3-WT, -L718P, -D723H and -T562N) were seeded on 100 μg/ml fibrinogen-coated coverslips in 6-well dishes. The cells, treated with or without RGDS, were stained with FITC-conjugated PAC-1 antibody and PerCP-conjugated anti-CD61 antibody and analysed by flow cytometry. (D) Activation index of αIIbβ3 mutants. Activation status of CHO cells expressing αIIbβ3-L718P and -D723H was compared with that of αIIbβ3-T562N as described in the "*Materials and methods*".

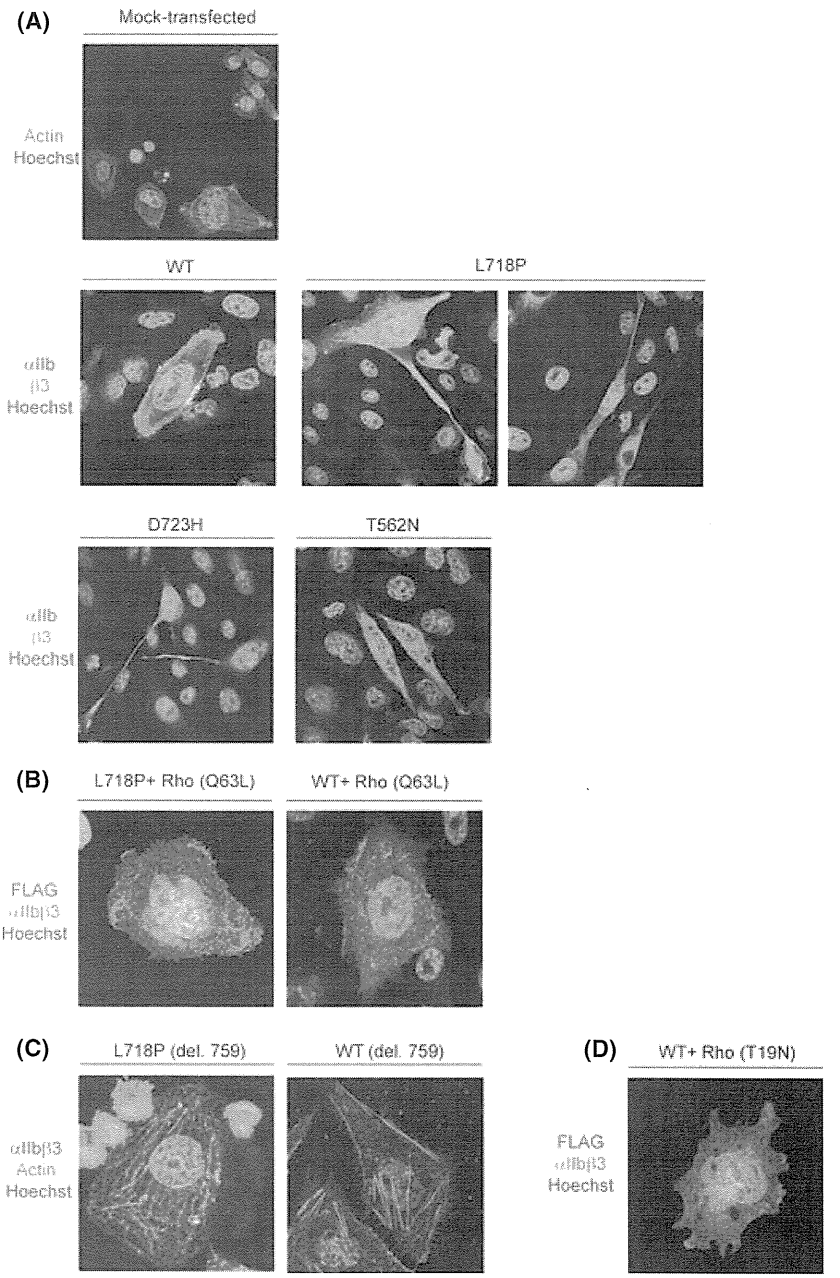

Fig 4. Overexpression of RhoA mutants or integrin β3-L718P (del. 759) modulates the formation of proplatelet-like cell protrusions in CHO cells. (A) Changes in CHO cell morphology by αIIbβ3 mutants. CHO cells transfected with αIIbβ3-L718P, -T562N and -D723H were seeded on fibrinogen-coated coverslips. After an 8-h incubation, the cells were fixed and stained with anti-CD41 and -CD61 antibodies followed by staining with Cy3- and Alexa 488-conjugated secondary antibodies. Mock-transfected cells were stained with Alexa 488-conjugated phalloidin and Hoechst 33342. (B) Inhibition of proplatelet-like protrusion formation by constitutively-active RhoA. An expression vector that encodes FLAG-tagged RhoA (Q63L) was transfected together with αIIbβ3-L718P or -WT expressing vectors into CHO cells. The cells grown on fibrinogen-coated coverslips were fixed and stained with anti-CD41 and anti-DDDDK-tag antibodies followed by staining with Alexa 488- and Cy3-conjugated secondary antibodies. (C) C-terminal deletion of β3-L718P inhibits the formation of proplatelet-like protrusions. C-terminal deleted integrin β3-L718P or -WT (del. 759) was expressed together with αIIb in CHO cells. The cells were fixed and stained with anti-CD41 antibody followed by staining with Cy3-conjugated secondary antibody and Alexa-488-labeled phalloidin. (D) A dominant-negative (T19N) form of RhoA was overexpressed in CHO cells. Images were taken as in (B).

Involvement of RhoA signalling in proplatelet-like protrusion formation

As previously reported by others (Ghevaert *et al*, 2008; Jayo *et al*, 2010), CHO cells expressing αIIbβ3-L718P, as well as αIIbβ D723H, formed long proplatelet-like protrusions on fibrinogen-coated dishes that were not observed in cells expressing wild-type αIIbβ3 (Fig 4A). In contrast, although cells expressing αIIbβ3-T562N, which yields a fully activated conformation (Kashiwagi *et al*, 1999), changed from their original round shape surrounded by a broad protrusion (Fig 4A, mock-transfected) to rhomboid-like cell morphology, proplatelet-like protrusions were rarely seen (Fig 4A). This suggests that mutants partially activating the integrin complex induce long proplatelet-like protrusions.

Recently, it was reported that the formation of proplatelet-like protrusions in CHO cells is mediated by the downregulation of RhoA activity (Chang *et al*, 2007; Schaffner-Reckinger *et al*, 2009), which is initiated by the binding of c-Src to the C-terminal tail (amino acid 760–762, Arg-Gln-Thr; RGT) of integrin β3 (Flevaris *et al*, 2007). We found that the formation of long cell protrusions was inhibited when a constitutively-active form of RhoA (Q63L) was introduced into αIIbβ3-L718P-expressing cells (Fig 4B). In addition, CHO cells expressing αIIbβ3-L718P (del. 759) mutant, which lacks the C-terminal c-Src binding site of in-

tegrin β3 (RGT), did not form any proplatelet-like protrusions (Fig 4C). Given that enforced activation of RhoA caused by introducing RhoA (Q63L), as well as de-repression of RhoA through C-terminal deletion of β3 in cells expressing αIIbβ3-WT, did not induce morphological changes in CHO cells (Figs 4B, C), it is proposed that constitutive inhibition but not activation through the c-terminal of β3 is responsible for the formation of abnormal cell protrusions in L718 mutants. However, as the enforced expression of a dominant negative form of RhoA (T19N) in αIIbβ3-WT expressing cells did not result in typical proplatelet-like protrusions (Fig 4D), this suggests that downregulation of RhoA was required but not sufficient for the formation of proplatelet-like protrusions induced by integrin β3-L718P.

Discussion

We report a pedigree with individuals suffering from a lifelong haemorrhagic syndrome, all of whom were carrying the integrin β3-L718P mutation. This had previously been reported only in a sporadic patient (Jayo *et al*, 2010). Next-generation sequencing, together with the clinical data of the patients, established that this integrin β3-L718P mutation causes thrombocytopenia resembling the disease caused by a different integrin mutation, β3-D723H, although the size of the platelets seems to differ somewhat between these mutations (Ghevaert *et al*, 2008; Schaffner-Reckinger *et al*, 2009).

Considering the dominant inheritance pattern of the haemorrhagic tendency caused by integrin β3-L718P as well as β3-D723H, these would be gain of function mutations, unlike those causing Glanzmann thrombasthenia. Indeed, expression of integrin β3-D723H partially activates the αIIbβ3 complex, resulting in downregulation of RhoA activity and induction of microtubule-dependent proplatelet-like cell protrusions considered relevant for production of macrothrombocytes (Ghevaert *et al*, 2008; Schaffner-Reckinger *et al*, 2009). Integrin β3-L718P appears to act in a similar fashion (Fig 4A and B). Interestingly, we demonstrate that the three C-terminal amino acid residues (RGT) of integrin β3 are required for L718P to form proplatelet-like cell protrusions (Fig 4C). RGT provides a binding site for c-Src tyrosine kinase, which was shown to inactivate RhoA (Flevaris *et al*, 2007), further supporting the hypothesis that integrin β3-L718P plays a role in causing megakaryocytes to produce abnormal platelets through the inhibition of RhoA.

In platelets derived from megakaryocytes that carry the integrin β3-L718P mutation, full activation of αIIbβ3 complex in response to inside-out stimuli is inhibited, as shown by reduced binding of PAC-1 and fibrinogen on stimulation with ADP (Fig 3B). A simple scenario is that, in platelets, integrin β3-L718P acts as a loss of function mutation. However, given that the carriers of Glanzmann's thrombasthenia who have both normal and mutant allele and express reduced amounts of the αIIbβ3 complex, in general show normal platelet aggregation, it is possible that the integrin β3-L718P mutation gains a function that ultimately results in the reduction of inside-out signals.

In summary, identification of a pedigree showing autosomal dominant inheritance leads to a model whereby the integrin β3-L718P mutation contributes to thrombocytopenia accompanied by anisocytosis most likely through gain-of-function mechanisms. Further investigations are necessary to fully elucidate these mechanisms by which this mutation exerts its abnormal effect on thrombocytosis and platelet aggregation.

Acknowledgements

We thank Prof. M. Matsumoto and Ms. M. Sasatani for providing clinical data; Ms. M. Nakamura, Ms. E. Kanai and Ms. R. Tai for excellent technical assistance. This work was partly supported by Grants-in-Aid for Scientific Research from the Ministry of Health, Labour and Welfare of Japan.

Author contributions

H.M., T.I. and M.K. designed the work. Y.K., H.M., A.K., S.O. and M.T. performed experiments and analysed data. S.K. contributed essential materials and interpreted data. M.M and K.N. contributed clinical materials and data. H.M, Y.K. and T.I. wrote the manuscript.

Conflict of interest

The authors declare no competing financial interests.

References

Chang, Y., Auradé, F., Larbret, F., Zhang, Y., Couedic, J.P.L., Momeux, L., Larghero, J., Bertoglio, J., Louache, F., Cramer, E., Vainchenker, W. & Debili, N. (2007) Proplatelet formation is regulated by the Rho/ROCK pathway. *Blood*, **109**, 4229–4236.

Flevaris, P., Stojanovic, A., Gong, H., Chishti, A., Welch, E. & Du, X. (2007) A molecular switch that controls cell spreading and retraction. *Journal of Cell Biology*, **179**, 553–565.

George, J.N., Caen, J.P. & Nurden, A.T. (1990) Glanzmann's thrombasthenia: the spectrum of clinical disease. *Blood*, **75**, 1383–1395.

Ghevaert, C., Salsmann, A., Watkins, N.A., Schaffner-Reckinger, E., Rankin, A., Garner, S.F., Stephans, J., Smith, G.A., Debili, N., Vainchenker, W.de, Groot, P.G., Huntington, J.A., Laffan, M., Kieffer, N. & Ouwehand, W.H. (2008) A non-synonymous SNP in the ITGB3 gene disrupts the conserved membrane-proximal cytoplasmic salt bridge in the αIIbβ3 integrin and cosegregates dominantly with abnormal proplatelet formation and macrothrombocytopenia. *Blood*, **111**, 3407–3414.

Hughes, P.E., Diaz-Gonzalez, F., Leong, L., Wu, C., McDonald, J.A., Shattil, S.J. & Ginsberg, M.H. (1996) Breaking the integrin hinge. A defined structural constraint regulates integrin signaling. *Journal of Biological Chemistry*, **271**, 6571–6574.

Jayo, A., Conde, I., Lastres, P., Martinez, C., Rivera, J., Vicente, V. & Manchón, C.G. (2010) L718P mutation in the membrane-proximal

cytoplasmic tail of β3 promotes abnormal αIIbβ3 clustering and lipid domain coalescence, and associates with a thrombasthenia-like phenotype. *Haematologica*, **95**, 1158–1166.

Kashiwagi, H., Tomiyama, Y., Tadokoro, S., Honda, S., Shiraga, M., Mizutani, H., Honda, M., Kurata, Y., Matsuzawa, Y. & Shattil, S.J. (1999) A mutation in the extracellular cysteine-rich repeat region of the β3 subunit activates integrins αIIbβ3 and αVβ3. *Blood*, **93**, 2559–2568.

Kunishima, S., Kashiwagi, H., Otsu, M., Takayama, N., Eto, K., Onodera, M., Miyajima, Y., Takamatsu, Y., Suzumiya, J., Matsubara, K., Tomiyama, Y. & Saito, H. (2011) Heterozygous ITGA2B R995W mutation inducing constitutive activation of the αIIbβ3 receptor affects proplatelet formation and causes congenital macrothrombocytopenia. *Blood*, **117**, 5479–5484.

Nurden, A.T. (2006) Glanzmann thrombasthenia. *Orphanet Journal of Rare Diseases*, **1**, 10.

Nurden, P. & Nurden, A.T. (2008) Congenital disorders associated with platelet dysfunctions. *Thrombosis and Haemostasis*, **99**, 253–263.

Nurden, A.T., Fiore, M., Nurden, P. & Pillois, X. (2011a) Glanznmann thrombasthenia: a review of ITGA2B and ITGB3 defects with emphasis on variants, phenotype variability, and mouse models. *Blood*, **118**, 5996–6005.

Nurden, A.T., Pillois, X., Fiore, M., Heilig, R. & Nurden, P. (2011b) Glanzmann thrombasthenia-like syndromes associated with macrothrombocytopenias and mutations in the gene encosing the αIIbβ3 integrin. *Seminars in Thrombosis and Hemostasis*, **37**, 698–706.

Schaffner-Reckinger, E., Salsmann, A., Debili, N., Bellis, J., Demey, J., Vainchenker, W., Ouwehand, W.H. & Kieffer, N. (2009) Overexpression of the partially activated αIIbβ3D723H integrin salt bridge mutant downregulates RhoA activity and induces microtubule-dependent proplatelet-like extensions in Chinese hamster ovary cells. *Journal of Thrombosis and Haemostasis*, **7**, 1207–1217.

Shattil, S.J., Cunningham, M. & Hoxie, J.A. (1987) Detection of activated platelets in whole blood using activation-dependent monoclonal antibodies and flow cytometry. *Blood*, **70**, 307–315.

Bone Marrow Transplantation (2013) **48,** 737–739

www.nature.com/bmt

LETTER TO THE EDITOR

Recipient seropositivity for adenovirus type 11 (AdV11) is a highly predictive factor for the development of AdV11-induced hemorrhagic cystitis after allogeneic hematopoietic SCT

Bone Marrow Transplantation (2013) **48,** 737–739; doi:10.1038/bmt.2012.206; published online 29 October 2012

Late-onset hemorrhagic cystitis (HC) is one of the most troublesome complications in patients undergoing allogeneic hematopoietic SCT (HSCT). As adenovirus serotype 11 (AdV11) with striking tropism for the urinary system is a pathogen predominantly responsible for late-onset HC after allogeneic HSCT in Japan,[1,2] it is important to assess the risk of AdV-HC and to make a rapid diagnosis of HC for early intervention.

Sixty-nine patients who underwent the first allogeneic HSCT between April 2005 and December 2006 were enrolled before the start of preparative conditioning. Standard urinalysis was performed at least once a week from 2 weeks before HSCT up to 3 months post HSCT and at the outpatient clinic every 2 or 4 weeks thereafter until 1 year post HSCT. In this study, late-onset HC was defined as HC that occurred 10 days after completion of the preparative

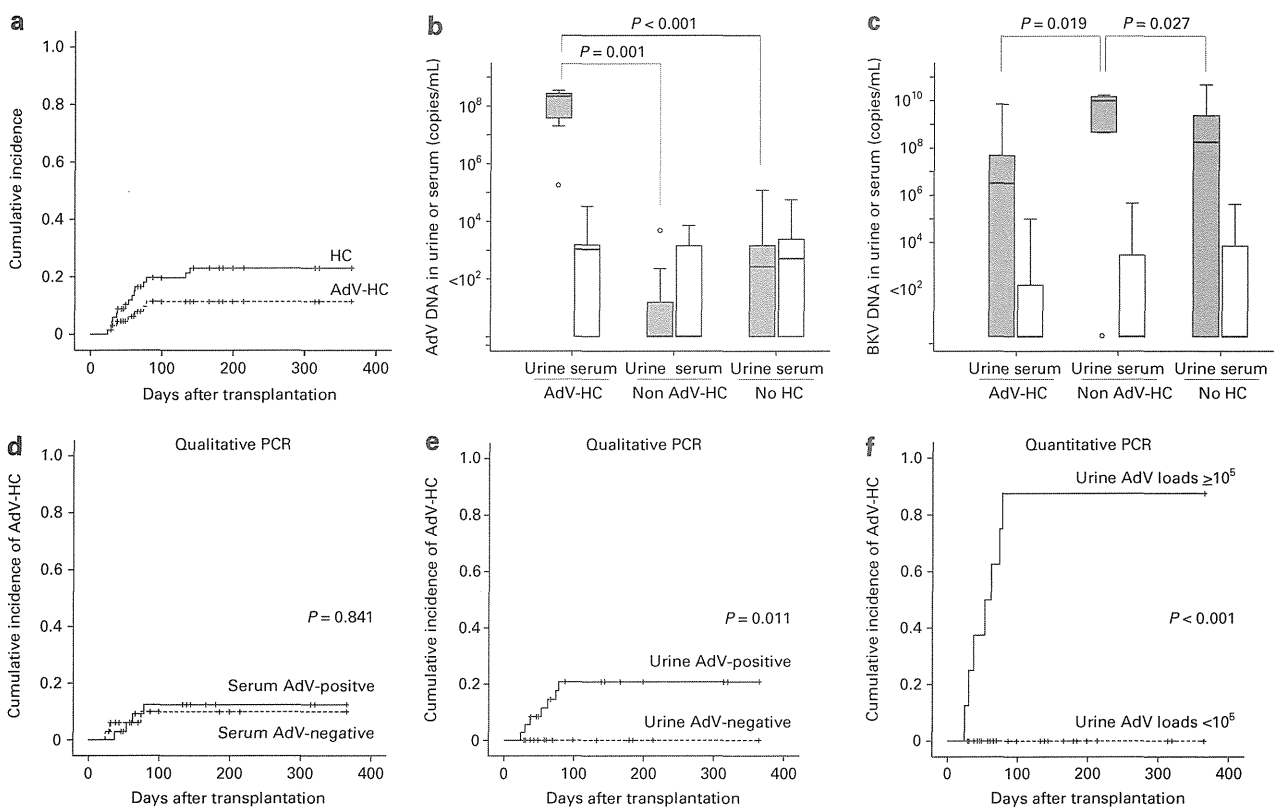

Figure 1. Cumulative incidence and viral loads of late-onset HC after allogeneic HSCT. (**a**) Cumulative incidence of late-onset HC and AdV-HC. In the Kaplan–Meyer curves, death without incidence of HC was defined as a competing event. The cumulative incidence of late-onset HC (solid line) over intervals from the start of allogeneic HSCT to the first day of hematuria was 23%, with a median interval after HSCT of 53 days (range: 24–139 days). The cumulative incidence of AdV-HC (dashed line) was 11%, with a median interval after HSCT of 53 days (range: 24–78 days). (**b**) Comparison of urinary and serum AdV loads among patients with HC from whom AdV was isolated by viral culture (AdV-HC), patients with HC from whom AdV was not isolated by viral culture (non-AdV-HC), and patients without HC (no HC). (**c**) Comparison of urinary and serum BKV loads among AdV-HC, non-AdV-HC and no HC group. The detection limit of the assay for both serum and urine was 1.0×10^2 copies/mL. To determine the significance of differences between two independent groups, the Mann–Whitney U-test was used. Only *P*-values showing statistical differences are presented. (**d–f**) Comparison of cumulative incidence of AdV-HC between qualitative PCR and quantitative PCR. The Kaplan–Meyer curves were compared using the log-rank test. (**d**) The cumulative incidence was 12.4% in patients with sera positive for AdV (solid line) and 9.9% in patients with sera negative for AdV (dashed line) according to the qualitative PCR. (**e**) The cumulative incidence was 20.8% in patients with urine positive for AdV (solid line) and 0% in patients with urine negative for AdV (dashed line) according to the qualitative PCR. (**f**) The cumulative incidence was 87.5% in patients with 1.0×10^5 copies/mL or higher of urine AdV loads (solid line) and 0% in patients with less than 1.0×10^5 copies/mL (dashed line) of urine AdV loads according to the quantitative PCR.

treatment. According to the published criteria,[3] we recorded grade 2 or higher HC as a clinically important complication in HSCT patients and performed viral cultures of their urine. As Akiyama *et al.*[2] reported that the viral culture is equivalent to PCR for diagnosis of AdV-HC, we classified HC into AdV-HC and non-AdV-HC based on the culture results. Among 69 subjects, 15 patients developed late-onset HC during the 1-year follow-up period (Figure 1a). Twenty-eight (40.6%) of 69 patients developed moderate or severe acute GVHD. Thirty-six patients (52.2%) were treated with corticosteroids for post-transplant complications such as engraftment syndrome and acute GVHD. The occurrence of acute GVHD was strongly associated with the incidence of HC according to the χ^2-test ($P<0.001$). Patients treated with corticosteroids developed HC more often than those not treated with corticosteroids, although this trend did not reach statistical significance ($P=0.064$). AdVs were cultured from the urine of 7 of

Table 1. Analysis of pre-transplant risk factors for development of late-onset HC: (a) univariate analysis (b) multivariate analysis

Variable	*Number of patients (n = 69)*	Number of patients with HC (AdV-HC)	P
Univariate analysis[a]			
Age[a]			
⩾16 years	27	9 (5)	0.061
<16 years	42	6 (2)	
Sex			
Male	45	12 (5)	0.174
Female	24	3 (2)	
Disease status[b]			
Advanced (non-CR)	27	8 (4)	0.203
Stable (CR or non-malignant)	42	7 (3)	
AdV11 serostatus of recipients[c]			
Positive	11	6 (6)	0.009
Negative	54	8 (1)	
Donor type[d]			
2- or 3-Ag mmRel or unrelated	48	13 (6)	0.104
Matched or 1-Ag mmRel	21	2 (1)	
Conditioning regimen[e]			
3-12Gy TBI-containing	56	11 (5)	0.458
No TBI	15	4 (2)	
Bu-containing	13	6 (2)	0.028
No Bu	56	9 (5)	
Cy-containing	46	8 (3)	0.216
No Cy	23	7 (4)	
Mel-containing	14	3 (2)	1.000
No Mel	55	12 (5)	
Flu-containing	31	7 (4)	0.878
No Flu	38	8 (3)	
ATG/ALG-containing	8	2 (1)	1.000
No ATG/ALG	61	13 (6)	
GVHD prophylaxis			
FK + MTX ± mPSL	50	10 (4)	0.745
CsA ± MTX	19	5 (3)	

Variables	*Unfavorable factors*	*Multivariate analysis*	
		Hazard ratio (95% CI)	P
Multivariate analysis[f]			
AdV11 antibody	Seropositive	7.87 (2.54 – 24.4)	<0.001
Sex	Male	4.54 (0.99 – 20.8)	0.051
Bu-containing	Used as conditioning	2.87 (0.94 – 8.77)	0.064
Donor type	2 or 3-Ag mmRel or unrelated	—	0.350
Age	⩾16 years	—	0.825

Abbreviations: AdV11, adenovirus serotype 11; ATG/ALG, anti-thymocyte/lymphocyte globulin; CI, confidence interval; FK, tacrolimus; Flu, fludarabine; HC, hemorrhagic cystitis; Mel, melphalan; mPSL, methylprednisolone; mmRel, mismatched relative. [a]Parameters from the patients' pre-transplant information were analyzed with the χ^2-test or Fisher's exact test. Statistical significance was defined as $P<0.05$. [b]Sixty patients had hematologic malignancies, four aplastic anemia, two primary immunodeficiencies and three metabolic disorders. [c]AdV11 serostatus was determined by a neutralizing antibody test using patient sera obtained before the start of preparative treatment. A result of 1:4 or higher was considered positive. Not tested in four recipients. [d]Sixteen patients underwent transplants from HLA-matched relatives, five from singe-antigen mismathced and eight from two- or three-mismatced relatives. Forty patients received grafts from unrelated donors (bone marrow in 30 and cord blood in 10). [e]The conditioning regimen was TBI + CY ± others in 40 patients, TBI + Mel ± others in 9 patients,TBI + Bu ± others in 7 patients. Bu + CY ± others in 3 patients, Bu + Flu ± others in 3 patients, non-TBI + non-Bu in 7 patients. [f]Parameters for which $P<0.2$ in the univariate analysis of pre-transplant information were applied to Cox regression model. Statistical significance was defined as $P<0.05$.

15 patients with late-onset HC and all strains were identified as AdV11. To examine the relationship between viral load and development of late-onset HC in patients undergoing allogeneic HSCT, we performed quantitative PCR for AdV and BK virus (BKV) in all serum and urine samples collected every 1 to 2 weeks after HSCT upto 180 days after HSCT. Primers and probe for identification of all serotypes of AdV and those for identification of BKV were designed, based on the reports described previously.[4–5] As presented in Figure 1b, the urine AdV loads at the onset of HC in the 7 patients with AdV-HC were markedly higher than the maximum values in the 8 patients with non-AdV-HC or the 54 patients without HC. There was no significant difference in the serum AdV loads among the AdV-HC, non-AdV-HC and no HC group. Lion *et al.*[6] presented the data that the incidence of AdV viremia in patients with AdV at above 1×10^6 copies/g of stool was significantly higher than in those with AdV levels in stool specimens below this threshold, suggesting that increase of stool AdV load predicts viremia. Accordingly, we investigated the data set for urine and blood. Among seven AdV-HC patients, four patients with AdV viremia (1.1×10^3 to 3.3×10^4 copies/mL) had 1.8×10^5 to 3.3×10^8 copies/mL of urine AdV loads, whereas 3 patients with no AdV viremia had 2.0×10^7 to 2.8×10^8 copies/mL of urine AdV loads. The cumulative incidence of AdV-HC was substantially different between qualitative PCR and quantitative PCR (Figures 1d–f). In particular, when AdV at 1.0×10^5 or higher copies/mL was detected in the urine, AdV-HC was diagnosed with 100% sensitivity, 98% specificity, 88% positive predictive value and 100% negative predictive value. On the other hand, qualitative PCR in urine samples displayed 100% sensitivity, 52% specificity, 19% positive predictive value, and 100% negative predictive value. Serial analyses in four of seven patients who developed AdV-HC revealed that adenoviruria reached $>1.0 \times 10^4$ copies/mL 1–2 weeks before the onset of HC. Accordingly, quantification of the urine AdV load may be more useful for diagnosing AdV-HC than qualitative PCR positivity.

As seven of eight non-AdV-HC patients had significant high urine BKV load between 4.3×10^8 and 1.7×10^{10} copies/mL (Figure 1c), most of the non-AdV-HC was considered to be BKV-associated HC. Among seven AdV-HC patients, three patients had concomitant BKV infections because of over a diagnostic viral load in urine (4.2×10^7 to 7.2×10^9 copies/mL) according to the criteria described by Cesaro *et al.*[7] The serum BKV load did not influence the development of HC. Therefore, BKV might be an alternative main cause of HC in Japan.

To identify factors predictive of the occurrence of late-onset HC, we first performed univariate analysis of the patients' pre-transplant information (Table 1a). Five factors (age, sex, recipient AdV11 serostatus, type of donor and conditioning regimen with or without Bu) showed $P<0.2$. Multivariate analysis revealed that recipient AdV11-seropositivity was the only significant risk factor (Table 1b).

HSCT-related AdV-HC is more frequent in Japan than in other countries (0–4%).[3,7,8] Several retrospective Japanese studies have reported risk factors including acute GVHD and chronic GVHD.[1,2,9,10] The influence of seropositivity for AdV was controversial.[1,2,9,10] In this study, we used a neutralizing antibody test to detect anti-AdV11 antibodies because this test is serotype-specific and can detect IgG antibodies for longer period after primary infection than can the complement fixation test. This prospective study revealed that the cumulative incidence of AdV-HC was 64% in the seropositive patients, but only 2% in the seronegative patients (log-rank test, $P<0.001$). Accordingly, recipient AdV11 serostatus is suggested to be the sole predictor of late-onset HC in Japanese allogeneic HSCT patients. Therefore, patients seropositive for AdV11 may be candidates for prophylactic anti-AdV treatment. It is likely that AdV-HC occurs in approximately 90% of allogeneic HSCT patients when the urine AdV load reached 1.0×10^5 copies/mL or more. Taken together with the finding of the time-course study, preemptive treatment may be recommended to begin when the urine AdV load reaches 1.0×10^4 copies/mL or higher.

CONFLICT OF INTEREST

The authors declare no conflict of interest.

ACKNOWLEDGEMENTS

YN was supported in this work by the Mother and Child Health Foundation (Osaka, Japan). We thank Dr Ritsuro Suzuki for his helpful advice.

Y Nakazawa[1], S Saito[1], R Yanagisawa[1], T Suzuki[2], T Ito[3], F Ishida[3], H Muramatsu[4], K Matsumoto[4], K Kato[4], H Ishida[5], K Umeda[6], S Adachi[6], T Nakahata[6] and K Koike[1]
[1]*Department of Pediatrics, Shinshu University School of Medicine, Matsumoto, Japan;*
[2]*Laboratory Medicine, Shinshu University Hospital, Matsumoto, Japan;*
[3]*Department of Hematology, Shinshu University School of Medicine, Matsumoto, Japan;*
[4]*Division of Hematology and Oncology, Children's Medical Center, Japanese Red Cross Nagoya First Hospital, Nagoya, Japan;*
[5]*Department of Pediatrics, Matsushita Memorial Hospital, Moriguchi, Japan and*
[6]*Department of Pediatrics, Graduate School of Medicine, Kyoto University, Kyoto, Japan*
E-mail: yxnakaza@shinshu-u.ac.jp

REFERENCES

1 Miyamura K, Takeyama K, Kojima S, Minami S, Matsuyama K, Morishima Y *et al.* Hemorrhagic cystitis associated with urinary excretion of adenovirus type 11 following allogeneic bone marrow transplantation. *Bone Marrow Transplant* 1989; **4**: 533–535.
2 Akiyama H, Kurosu T, Sakashita C, Inoue T, Mori Si, Ohashi K *et al.* Adenovirus is a key pathogen in hemorrhagic cystitis associated with bone marrow transplantation. *Clin Infect Dis* 2001; **32**: 1325–1330.
3 Bedi A, Miller CB, Hanson JL, Goodman S, Ambinder RF, Charache P *et al.* Association of BK virus with failure of prophylaxis against hemorrhagic cystitis following bone marrow transplantation. *J Clin Oncol* 1995; **13**: 1103–1109.
4 Heim A, Ebnet C, Harste G, Pring-Akerblom P. Rapid and quantitative detection of human adenovirus DNA by real-time PCR. *J Med Virol* 2003; **70**: 228–239.
5 McNees AL, White ZS, Zanwar P, Vilchez RA, Butel JS. Specific and quantitative detection of human polyomaviruses BKV, JCV, and SV40 by real time PCR. *J Clin Virol* 2005; **34**: 52–62.
6 Lion T, Kosulin K, Landlinger C, Rauch M, Preuner S, Jugovic D *et al.* Monitoring of adenovirus load in stool by real-time PCR permits early detection of impending invasive infection in patients after allogeneic stem cell transplantation. *Leukemia* 2010; **24**: 706–714.
7 Cesaro S, Facchin C, Tridello G, Messina C, Calore E, Biasolo MA *et al.* A prospective study of BK-virus-associated haemorrhagic cystitis in paediatric patients undergoing allogeneic haematopoietic stem cell transplantation. *Bone Marrow Transplant* 2008; **41**: 363–370.
8 Azzi A, Fanci R, Bosi A, Ciappi S, Zakrzewska K, de Santis R *et al.* Monitoring of polyomavirus BK viruria in bone marrow transplantation patients by DNA hybridization assay and by polymerase chain reaction: an approach to assess the relationship between BK viruria and hemorrhagic cystitis. *Bone Marrow Transplant* 1994; **14**: 235–240.
9 Yamamoto R, Kusumi E, Kami M, Yuji K, Hamaki T, Saito A *et al.* Late hemorrhagic cystitis after reduced-intensity hematopoietic stem cell transplantation (RIST). *Bone Marrow Transplant* 2003; **32**: 1089–1095.
10 Mori Y, Miyamoto T, Kato K, Kamezaki K, Kuriyama T, Oku S *et al.* Different risk factors related to adenovirus- or BK virus-associated hemorrhagic cystitis following allogeneic stem cell transplantation. *Biol Blood Marrow Transplant* 2012; **18**: 458–465.

Regular Article

MYELOID NEOPLASIA

Clonal selection in xenografted TAM recapitulates the evolutionary process of myeloid leukemia in Down syndrome

Satoshi Saida,[1] Ken-ichiro Watanabe,[1] Aiko Sato-Otsubo,[2] Kiminori Terui,[3] Kenichi Yoshida,[2] Yusuke Okuno,[2] Tsutomu Toki,[3] RuNan Wang,[3] Yuichi Shiraishi,[4] Satoru Miyano,[4] Itaru Kato,[1] Tatsuya Morishima,[1] Hisanori Fujino,[1] Katsutsugu Umeda,[1] Hidefumi Hiramatsu,[1] Souichi Adachi,[5] Etsuro Ito,[3] Seishi Ogawa,[2] Mamoru Ito,[6] Tatsutoshi Nakahata,[7] and Toshio Heike[1]

[1]Department of Pediatrics, Graduate School of Medicine, Kyoto University, Kyoto, Japan; [2]Cancer Genomics Project, Graduate School of Medicine, University of Tokyo, Tokyo, Japan; [3]Department of Pediatrics, Graduate School of Medicine, Hirosaki University, Hirosaki, Japan; [4]Laboratory of DNA Information Analysis, Human Genome Center, Institute of Medical Science, University of Tokyo, Tokyo, Japan; [5]Department of Human Health Sciences, Graduate School of Medicine, Kyoto University, Kyoto, Japan; [6]Laboratory Animal Research Department, Central Institute for Experimental Animals, Kawasaki, Japan; and [7]Department of Clinical Application, Center for iPS Cell Research and Application, Kyoto University, Kyoto, Japan

Key Points

- Genetically heterogeneous subclones with varying leukemia-initiating potential exist in neonatal transient abnormal myelopoiesis.
- This novel xenograft model of transient abnormal myelopoiesis may provide unique insight into the evolutionary process of leukemia.

Transient abnormal myelopoiesis (TAM) is a clonal preleukemic disorder that progresses to myeloid leukemia of Down syndrome (ML-DS) through the accumulation of genetic alterations. To investigate the mechanism of leukemogenesis in this disorder, a xenograft model of TAM was established using NOD/Shi-*scid*, interleukin (IL)-2Rγ^{null} mice. Serial engraftment after transplantation of cells from a TAM patient who developed ML-DS a year later demonstrated their self-renewal capacity. A *GATA1* mutation and no copy number alterations (CNAs) were detected in the primary patient sample by conventional genomic sequencing and CNA profiling. However, in serial transplantations, engrafted TAM-derived cells showed the emergence of divergent subclones with another *GATA1* mutation and various CNAs, including a 16q deletion and 1q gain, which are clinically associated with ML-DS. Detailed genomic analysis identified minor subclones with a 16q deletion or this distinct *GATA1* mutation in the primary patient sample. These results suggest that genetically heterogeneous subclones with varying leukemia-initiating potential already exist in the neonatal TAM phase, and ML-DS may develop from a pool of such minor clones through clonal selection. Our xenograft model of TAM may provide unique insight into the evolutionary process of leukemia. (*Blood*. 2013;121(21):4377-4387)

Introduction

Neonates with Down syndrome (DS) are at high risk of developing a unique hematologic disorder referred to as transient abnormal myelopoiesis (TAM), transient myeloproliferative disorder, or transient leukemia. In most cases, TAM resolves spontaneously within 3 months.[1,2] However, after spontaneous remission, 20% of TAM patients develop myelodysplastic syndrome and acute megakaryocytic leukemia referred to as myeloid leukemia of DS (ML-DS) within 4 years.[3,4] Blast cells in most patients with TAM and ML-DS have mutations in exon 2 of the gene coding for the transcription factor *GATA1*,[5-8] which is essential for the normal development of erythroid and megakaryocytic cells.[9,10] Although blast cells in most TAM and ML-DS patients share the identical *GATA1* mutation, recurrent additional cytogenetic abnormalities are commonly observed during disease progression.[2,5,11,12] In fact, a ML-DS case derived from a minor clone with a distinct *GATA1* mutation in the TAM phase was previously reported by our group.[13] These clinical findings suggest that although most TAM cells disappear in the early neonatal phase, a few clones persist during apparent remission to develop ML-DS later. Because only one fifth of TAM cases progress to ML-DS, additional genetic events besides *GATA1* mutation are likely to be involved in the progression of TAM to ML-DS.[14] As mentioned above, the development of ML-DS is significantly correlated with karyotypic abnormalities such as duplication (dup)(1q), deletion (del)(6q), del(7p), dup(7q), +8, +11, and del(16q),[2,11,12] which are rarely observed in the TAM phase. These clinical findings have led many physicians to consider TAM as preleukemia and the progression of TAM to ML-DS as an attractive model to investigate multistep leukemogenesis.

Animal models have contributed to our understanding of the pathogenesis of TAM/ML-DS and other leukemias.[15-21] Mice models in which primary human leukemic cells were transplanted into immunodeficient hosts provided significant clues to advance our understanding of the pathogenesis of human leukemia.[19-22] However,

Submitted December 18, 2012; accepted February 4, 2013. Prepublished online as *Blood* First Edition paper, March 12, 2013; DOI 10.1182/blood-2012-12-474387.

The online version of this article contains a data supplement.

The publication costs of this article were defrayed in part by page charge payment. Therefore, and solely to indicate this fact, this article is hereby marked "advertisement" in accordance with 18 USC section 1734.

xenograft models of primary patient samples from the preleukemic phase have been rarely reported, and the TAM xenograft model would be an attractive method to investigate leukemogenesis.

We previously described the development of novel immunodeficient NOD/Shi-*scid*, interleukin (IL)-2Rγ^{null} (NOG) mice with a superior capacity for the engraftment of human hematopoietic and neoplastic cells.[23-26] In contrast to a previous study in which TAM cells showed a limited ability to expand in immunodeficient mice,[27] we established a xenograft model where TAM cells were transplanted into NOG mice to recapitulate the pathophysiology of TAM/ML-DS. This xenograft model in combination with high-throughput genomic technology was used to show that genetically heterogeneous minor subclones with leukemia-initiating potential already exist in the neonatal TAM phase and could serve as initiating clones evolving to ML-DS in a patient. Our TAM xenograft model may be of value to gain insight into the evolutionary process of leukemia.

Materials and methods

Patients and sample collection

Peripheral blood (PB) samples were obtained from patients diagnosed with TAM associated with DS in acute and complete remission phases. Mononuclear cells were separated by Ficoll-Hypaque (Pharmacia, Uppsala, Sweden) density gradient centrifugation, as previously described.[23] Informed consent was obtained from the patients' parents in accordance with the Declaration of Helsinki, and the research was approved by the institutional ethics committee of Kyoto University Hospital.

Mice

NOG mice were developed at the Central Institute of Experimental Animals (Kawasaki, Japan) as previously described[28] and were maintained in our pathogen-free facility and cared for in accordance with the institutional guidelines for animal welfare.

Primary and serial xenogeneic transplantation into NOG mice

Xenotransplantation and analysis of TAM cells were performed using a previously reported method with some modifications.[26] In brief, PB mononuclear cells (PBMCs) obtained from TAM patients ($1–3 \times 10^6$ cells) were injected into 2.4 Gy–irradiated 8- to 12-week-old NOG mice through the tail vein. To screen for the proliferation of TAM-derived cells, bone marrow (BM) cells were aspirated from the tibia every 4 weeks. Engraftment was defined as >1% of cells staining positive for human CD7 (hCD7), hCD33, hCD41a, hCD45, and hCD117 at 12 weeks after transplantation. For serial transplantation, recipient BM cells were collected 12 to 18 weeks after transplantation; the equivalent of 1×10^6 hCD45$^+$ cells was intravenously transplanted into new mice. For a detailed determination of chromosomal and genetic alterations in TAM-derived cells, serial transplantation experiments using preserved PBMC samples were performed.

Flow cytometric analysis of transplanted TAM-derived cells

For analysis of TAM-derived cells in murine BM, mice were euthanized, and the BM was removed and mechanically dispersed. Mononuclear cells were purified from the BM and stained with antibodies. Dead cells were excluded according to 4′,6-diamidino-2-phenylindole staining. Blast cells were identified by classical CD45/SSC blast gating.[29] See supplemental Methods on the *Blood* Web site for details.

Human cell sorting

Human cell isolation was performed according to a previously described method with some modifications.[23,24] See supplemental Methods for details.

Colony assay

Leukemic colony formation was assessed according to a previously described method with some modifications.[30] See supplemental Methods for details.

GATA1 genomic sequencing analysis

The *GATA1* gene was amplified using polymerase chain reaction (PCR) as previously described[8] and sequenced by an ABI 3130xl Genetic analyzer (Applied Biosystems, Foster City, CA).

DNA copy number analysis

DNA copy number analysis was performed using GeneChip Human Mapping 250K Nsp arrays (Affymetrix, Inc., Santa Clara, CA) according to the manufacturer's standard protocols. Genomic copy numbers including allele-specific copy numbers were calculated using CNAG/AsCNAR software (http://www.genome.umin.jp), and genomic DNA obtained from PB of patients in the remission phase was used as a control. Copy number abnormalities and other allelic imbalances were detected using a hidden Marcov model–based algorithm.

Statistical analysis

Data are presented as the mean ± standard deviation. The 2-sided P value was determined by testing the null hypothesis that the 2 population medians are equal. P values <0.05 were considered to be significant.

Results

Establishment of a TAM xenograft model using NOG mice

To determine whether NOG mice provide a TAM xenograft model, Ficoll-purified PB samples from 11 TAM patients were transplanted into irradiated NOG mice. Patient characteristics are shown in Table 1. Patients' ages at sample collection, percentage of blast cells, number of cells injected, and number of engrafted recipients for each PB sample are shown in supplemental Table 1. Of 11 patient samples, 3 (patients 1, 2, and 9) were engrafted successfully in the recipient mice. Engraftment was maintained ≥12 weeks in all cases (Figure 1A). The spleen and liver of the recipients were also infiltrated with hCD45$^+$ blast cells (data not shown). These TAM-derived cells were morphologically similar to the primary TAM cells obtained from the patients (Figure 1B). Flow cytometric analysis of surface antigens detected the expression of CD117, CD34, CD33, and CD41a on hCD45$^+$ cells, which was consistent with the pattern observed in primary cells of TAM patients (Figure 1C). The presence of the same *GATA1* mutation was confirmed in the primary TAM cells and the engrafted cells in NOG mice (Figure 1D; supplemental Table 1). Chromosomal analysis of engrafted cells showed no abnormalities other than trisomy 21 (Figure 1E). These TAM-derived cells were detectable in the recipient's BM for >24 weeks (data not shown).

NOG mice can support self-renewal of TAM-derived cells

To examine the self-renewal capacity of TAM-derived cells, we performed serial transplantation of engrafted cells in the BM of recipient mice. Only the TAM-derived cells from patient 1 were successfully engrafted into the secondary (2°) and tertiary (3°) recipients. The morphology and surface antigen expression of these engrafted cells remained unchanged throughout the serial transplantation (Figure 2A-B). Interestingly, the TAM-derived cells

Table 1. Clinical characteristics of 11 TAM patients

Patient no.	Gender	Period of gestation, wk	Weight at birth, g	PB at diagnosis of TAM				Cytogenetics International System for Human Cytogenetic Nomenclature (2009)	*GATA1* mutation	Treatment		Clinical outcome	Onset of ML-DS (m of age)	Follow-up interval
				WBC, $\times 10^3$/ μL	Blast, %	Hb, g/dL	Plt, $\times 10^3$/ μL			Exchange transfusion	Low-dose Ara-C			
1	F	36	3050	159	91	9.1	247	47,XX,+21 [20]	c.38_39delAG	No	Yes	Alive	Yes (14)	27
2	M	37	1868	45.0	65	19.0	80	47,XY,+21 [20]	c.49C>T	No	Yes	Alive	No	24
3	F	39	3102	40.3	37	15.1	304	47,XX,+21 [20]	c.59_174del116	No	No	Alive	No	23
4	M	37	2780	15.6	24	17.0	50	47,XY,+21 [20]	c.163_169del	No	No	Alive	No	22
5	M	39	3052	60.9	48	20.7	258	47,XY,+21 [19]	c.37G>T	No	No	Alive	No	21
6	F	37	2050	13.6	12	20.9	291	47,XX,+21 [20]	N/A	No	No	Alive	No	19
7	M	38	2694	280	87	13.6	26	47,XY,+21 [20]	c.186C>G	Yes	Yes	DOD	No	1
8	M	35	2070	174	80	19.2	117	47,XY,+21 [20]	c.-19-1G>A, c.1A>G	Yes	No	Alive	No	17
9	M	39	3380	56.2	65	20.2	156	47,XY,+21 [20]	c.35C>G	No	Yes	Alive	No	14
10	M	36	2131	199	84	12.2	73	47,XY,+21 [20]	c.19_20insCCTGA	Yes	Yes	Alive	No	14
11	F	33	2032	254	90	14.3	178	47,XX,+21 [20]	c.-19-62_-5delinsA	Yes	Yes	Alive	No	10

Brackets under International System for Human Cytogenetic Nomenclature indicate the number of analyzed cells in metaphase.
Ara-C, cytosine arabinoside; DOD, died of disease; Hb, hemoglobin; N/A, not assessed; Plt, platelet; WBC, white blood cell.

expanded rapidly in the 3° recipients (Figure 2C). The colony-forming ability of the engrafted cells also increased in subsequent generations (Figure 2D). These cells could be grown by serial transplantation for >1 year and ⩾8° recipients, indicating that some TAM clones had long-term self-renewal capacity, a characteristic of leukemia. Indeed, patient 1 developed ML-DS at the age of 1 year, whereas the other patients did not (Table 1).

TAM-NOG xenograft model recapitulates leukemic evolution from TAM

Additional chromosomal alterations are frequently observed in ML-DS in comparison with TAM, suggesting that these alterations in genomic structure could be related to the evolution of ML-DS from TAM.[2,11,12] Therefore, we first investigated whether the serially engrafted TAM-derived cells (from patient 1) had DNA copy number alterations (CNAs) using Affymetrix GeneChip Mapping 250K arrays. Primary samples from patient 1 had no CNAs other than the gain of chromosome 21. However, the TAM-derived cells in the 1° recipients showed heterozygous deletion of 16q22 and 16q24 (Figure 3). To determine whether these deletions were present in the same cell, we calculated the signal intensities of each deletion using array data. Nearly 100% of TAM-derived cells harbored each deletion, indicating that these 2 deletions exist in a single TAM-derived cell. Although 2° recipients showed the same CNAs, 3° recipients showed additional CNAs, namely the gain of the entire chromosome 1q (Figure 3; supplemental Figure 1A). Interestingly, the 1q gain was not detected in the 4° to 7° recipients, whereas deletions of 16q22 and 16q24 were present (Figure 3). In this series of transplantations, the original *GATA1* mutation found in the primary patient sample (patient 1) remained unchanged (supplemental Figure 1B).

Gain of 1q and deletions in 16q are recurrent chromosomal abnormalities in ML-DS.[11,12,31] The result of G-band karyotyping of TAM-derived cells in 3° recipients was 47,XX,+1, der (1;15)(q10;q10),+21 in 20/20 metaphase cells (supplemental Figure 1C), confirming genomic structural change, which is a hallmark of ML-DS. These data suggest that leukemic evolution of TAM-derived cells was observed in our NOG mouse model.

Genetically heterogeneous subclones with varying repopulating capacity expanded in the TAM-NOG xenograft model

To examine the kinetics of the leukemic evolution of TAM cells, another 2 sets of serial transplantations were performed using the preserved patient 1 sample (Figure 4A). Four of 5 mice in the second group (m2-1–m2-5) and 5 of 11 mice in the third group (m3-1–m3-11) harbored TAM cells from the patient. Of the total of 9 engrafted mice, 2 had the same CNAs detected in the first series of serial transplantations: deletion of 16q22 and 16q24 (m3-5 and m3-8; Figure 3). Moreover, 2 combinations of new CNAs were detected in the 1° recipients: deletion of 9q22 +12p12 (m3-4 and m3-7) and gain of 1q25.2-1q44 (m3-11). No CNAs other than the gain of chromosome 21 were detected in the other recipients (m2-1, m2-2, m2-4, and m2-5).

Each 1° engrafted mouse was subjected to 2° transplantation, and 5 of 9 series (m2-5, m3-4, m3-7, m3-8, and m3-11) successfully gave rise to the xenografts in the 2° recipients. It is noteworthy that the TAM-derived cells of the 2° recipients in 2 of the 3 analyzed series (m2-5 and m3-4) acquired additional CNAs, whereas the CNAs in 2 descendent 2° recipients of m3-8 remained unchanged. The additional CNA of gain of 1q was detected in the 2° recipients of m3-4, similar to that observed in the 3° recipient in Figure 3. Although

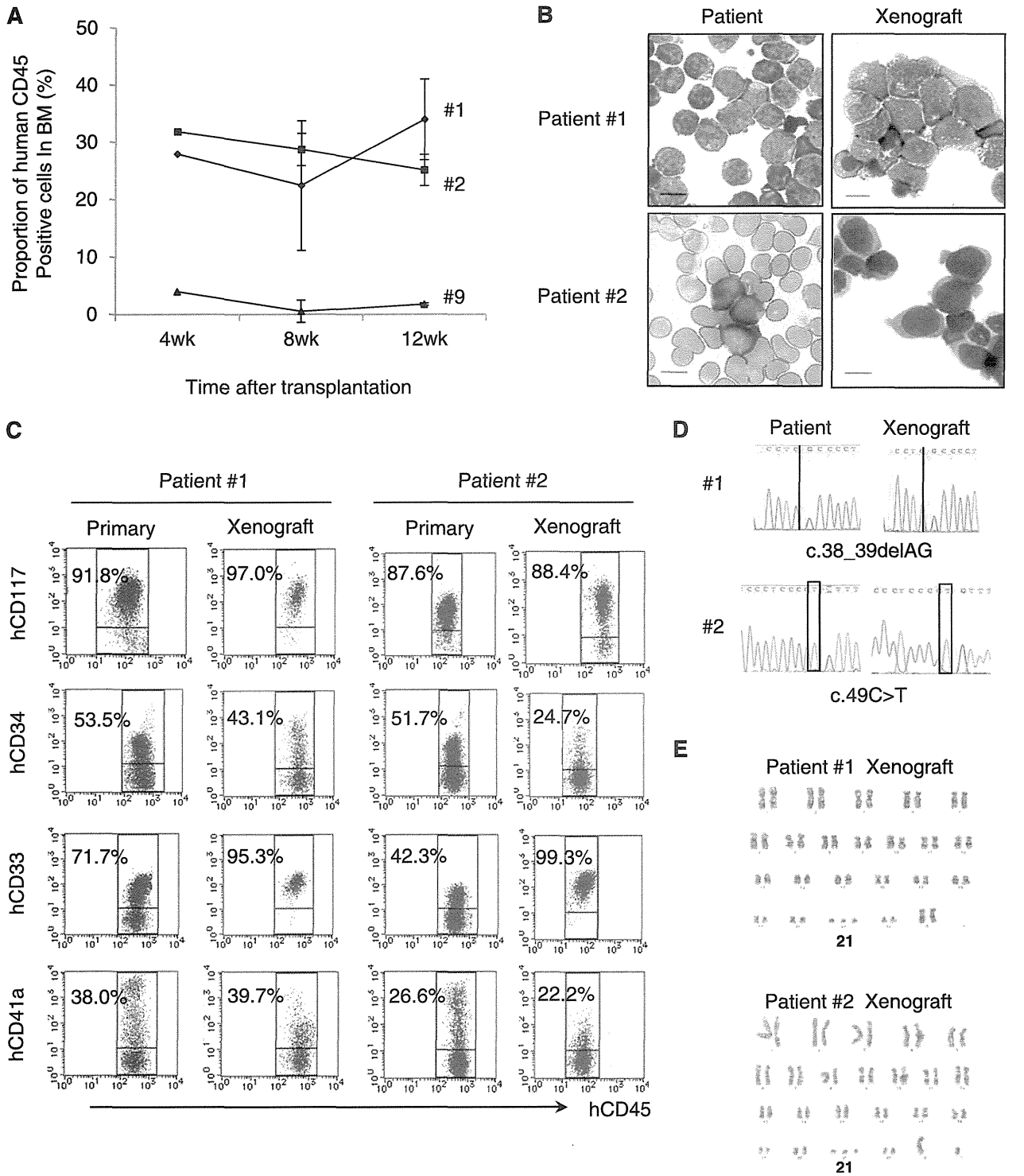

Figure 1. TAM cells engrafted in NOG mice. (A) Proportion of human CD45$^+$ cells in the BM of NOG mice at 4, 8, and 12 weeks after transplantation (n = 3–5 per group). (B) May-Giemsa staining of the BM smear of patients and cytospin preparation of human CD45$^+$ cells in the recipient NOG mice. Blast cells with cytoplasmic blebbing consistent with megakaryocytic differentiation were present in the BM of recipient mice. (C) Surface marker analysis of engrafted TAM cells. Human CD45$^+$ TAM-derived cells expressing hCD117, hCD34, hCD33, and hCD41a are detected in the recipient's BM. Blast cells were identified by CD45/SSC gating, and debris (low forward scatter) and dead cells (4′,6-diamidino-2-phenylindole positive) were excluded from the analysis. A representative result of >3 experiments is shown. (D) Genomic direct sequencing shows the presence of concordant GATA1 mutation in xenograft and original patients (1 and 2). (E) G-band karyotyping of TAM-derived cells in recipient murine BM shows no additional chromosome abnormality apart from constitutional trisomy 21, consistent with the findings in the original patients. The GATA1 mutation and the karyotype of engrafted cells from patient 9 were not assessed because of a low cell number.

gain of 1q was recurrently observed in this series, the duplicated regions were diverse: 1q25.2-1q44 (1°, m3-11), 1q21.3-1q44 (2°, m3-4), 1q31.2-1q44 (2°, m3-4), and the whole arm of chromosome 1q (3° in Figures 3 and 4A; supplemental Figure 2). In m2-5, a deletion of 3q24 appeared in the 2° and 3° recipients. These results demonstrated that TAM cells derived from patient 1

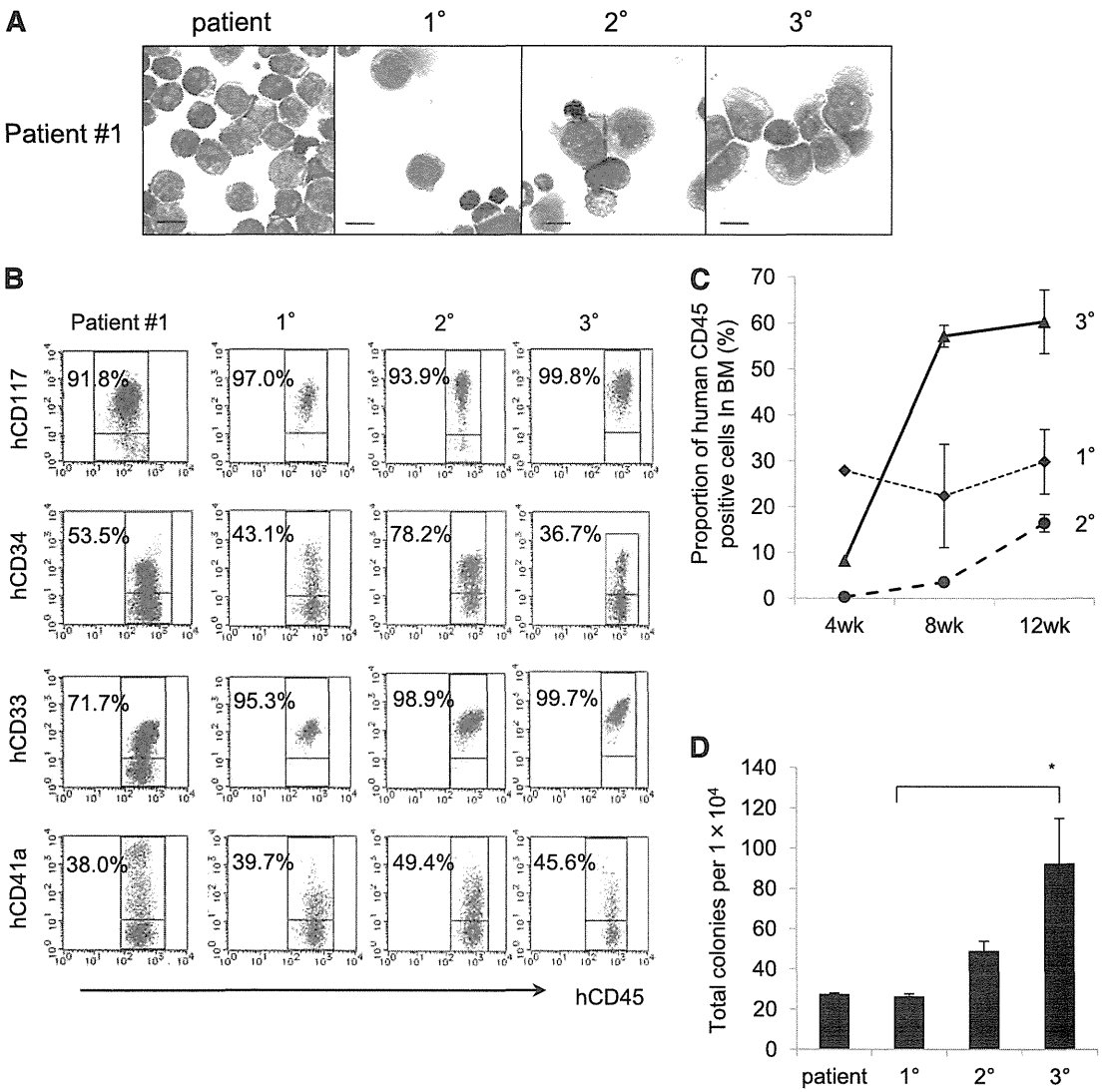

Figure 2. The NOG mouse model can support self-renewal of TAM-derived cells. (A) May-Giemsa staining of TAM-derived cells in recipients of patient 1. (B) Surface marker analysis of TAM-derived cells in recipients by flow cytometry. Viable cells were gated according to their forward scatter (FSC) and 4′,6-diamidino-2-phenylindole staining, blast cells were identified by CD45/SSC gating, and hCD45$^+$-gated cells were tested for the expression of hCD117, hCD34, hCD33, and hCD41a. (C) Proportion of hCD45$^+$ cells in BM of 1°, 2°, and 3° recipient mice at 4, 8, and 12 weeks after transplantation. (D) Colony assay of hCD45$^+$ cells in BM of 1°, 2°, and 3° recipient mice. hCD45$^+$ cells were seeded at 1.0×10^4 cells per 35-mm dish in triplicate, and the number of colonies in each dish was counted. Bars represent the standard deviation of the mean of 3 independent experiments. *Significant difference ($P < .05$).

acquired various CNAs and showed divergent repopulating capacity in our xenograft model.

TAM-NOG xenograft model revealed the presence of a minor clone with a distinct GATA1 mutation

ML-DS can arise from a minor TAM clone with a *GATA1* mutation that is distinct from that of the major TAM clone in a patient.[13] To determine whether the *GATA1* mutation in the primary patient's TAM cells was preserved in engrafted TAM-derived cells, *GATA1* mutation analysis was performed. TAM-derived cells in the series m3-4, m3-5, m3-7, and m3-8 had the same *GATA1* mutation (c.38_39delAG) as that of patient 1 (Figure 4A). Surprisingly, this mutation was not detected in TAM-derived cells in m2-1, m2-2, m2-5, and m3-11; instead, these samples showed a distinct *GATA1* mutation (c.1A>G) that was not detectable in the primary patient sample by direct sequencing. One of the 1° recipients (m2-4) showed both *GATA1* mutations. These results suggested that a minor clone with a distinct *GATA1* mutation (c.1A>G) was present in the primary patient sample and that this minor clone coexisted with, or predominated over, other clones in some 1° recipients. Therefore, a mutation-specific restriction enzyme digestion assay was performed using the primary sample from patient 1, which confirmed the presence of cells with the *GATA1* mutation (c.1A>G) as a minor clone (Figure 4B). Moreover, this minor clone propagated and acquired CNAs in NOG mice independently of the major clones (Figure 4A), further demonstrating the genetic heterogeneity of TAM cells. Interestingly, the major clone in the original patient 1 sample with a c.38_39delAG *GATA1* mutation and no CNAs did not become dominant in any of the recipients.

Minor subclone with additional CNAs was present in the primary TAM patient sample

TAM-derived cells in multiple 1° recipients derived from patient 1 had various CNAs including deletions of 16q22 and 16q24